JOURNAL OF PETROLOGY | VOLUME 47 | NUMBER 2 | PAGES 301–328 | 2006 | doi:10.1093/petrology/egi076

Generation of Porphyritic and Equigranular Mafic Enclaves During Magma Recharge Events at Unzen Volcano, Japan

BRANDON L. BROWNE[1]*, JOHN C. EICHELBERGER[1], LINA C. PATINO[2], THOMAS A. VOGEL[2], JONATHAN DEHN[1], KOZO UTO[3] AND HIDEO HOSHIZUMI[3]

[1]UNIVERSITY OF ALASKA FAIRBANKS, GEOPHYSICAL INSTITUTE, FAIRBANKS, AK 99775, USA

[2]MICHIGAN STATE UNIVERSITY, DEPARTMENT OF GEOLOGICAL SCIENCES, EAST LANSING, MI 48824, USA

[3]GEOLOGICAL SURVEY OF JAPAN, HIGASHI 1-1-3, TSUKUBA, IBARAKI 305-8567, JAPAN

RECEIVED MAY 26, 2004; ACCEPTED SEPTEMBER 1, 2005
ADVANCE ACCESS PUBLICATION SEPTEMBER 28, 2005

Mafic to intermediate enclaves are evenly distributed throughout the dacitic 1991–1995 lava sequence of Unzen volcano, Japan, representing hundreds of mafic recharge events over the life of the volcano. This study documents the morphological, textural, chemical, and petrological characteristics of the enclaves and coexisting silicic host lavas. The eruptive products described in this study appear to be general products of magma mingling, as the same textural types are seen at many other volcanoes. Two types of magmatic enclaves, referred to as Porphyritic and Equigranular, are easily distinguished texturally. Porphyritic enclaves display a wide range in composition from basalt to andesite, are glass-rich, spherical and porphyritic, and contain large, resorbed, plagioclase phenocrysts in a matrix of acicular crystals and glass. Equigranular enclaves are andesitic, non-porphyritic, and consist of tabular, medium-grained microphenocrysts in a matrix glass that is in equilibrium with the host dacite magma. Porphyritic enclaves are produced when intruding basaltic magma engulfs melt and phenocrysts of resident silicic magma at their mutual interface. Equigranular enclaves are a product of a more prolonged mixing and gradual crystallization at a slower cooling rate within the interior of the mafic intrusion.

KEY WORDS: *mafic enclaves; quenched mafic inclusions; magma mingling; Unzen volcano; Unzen Scientific Drilling Project; resorbed plagioclase*

INTRODUCTION

The 1991–1995 eruption of Unzen volcano claimed 44 lives and resulted in approximately US$2 billion in damage. In 1999, an interdisciplinary volcanological project of unprecedented scope, known as the Unzen Scientific Drilling Project (USDP), was initiated. Its purpose was to provide a new level of fundamental understanding of this type of volcanism, which has been dominated by effusive eruptions of crystal-rich dacite for the past ~500 kyr. The first phase of the project was coring through the erupted material at two flank holes (Hoshizumi *et al.*, 1999; Uto *et al.*, 2002) to understand the growth of the volcano and the evolution of its magma. The final phase was drilling and coring the recent magmatic conduit to understand eruptive processes, as part of the International Continental Drilling Program (ICDP). One important scientific issue that the USDP sought to address is how Unzen magmas form. Our particular contribution to the first phase of this project focuses on the mafic-to-intermediate enclaves that are widespread throughout Unzen's eruptive products, with the exception of a lava flow erupted in 1663.

The presence of chilled mafic enclaves, also described as 'under-cooled inclusions' (e.g. Bacon, 1986) in igneous rocks is well documented in andesitic to rhyolitic lava flows and domes (e.g. Eichelberger, 1978, 1980; Heiken & Eichelberger, 1980; Bacon & Metz, 1984; Singer *et al.*, 1995; Clynne, 1999; Davidson *et al.*, 2001), as well as in the plutonic record (e.g. Didier, 1973; Vernon, 1983, 1984; Wiebe, 1994; Wiebe & Collins, 1998; Wiebe *et al.*, 2002). The enclaves are interpreted to form by mingling in the liquid state of coexisting magmas with strongly

*Corresponding author. Present address: California State University, Fullerton, Department of Geological Sciences, Fullerton, CA 92834, USA. Telephone: +1 (714) 278-3054. Fax: +1 (714) 278-7266. E-mail: bbrowne@fullerton.edu

contrasting physical properties (Eichelberger *et al.*, 1976; Bacon, 1986; Sparks & Marshall, 1986; Stimac *et al.*, 1990; Koyaguchi & Blake, 1991; Stimac & Pearce, 1992), as indicated by textural evidence such as a spherical or ellipsoidal shape with vesicular interiors, acicular groundmass minerals and/or cuspate margins. The types and morphologies of enclaves in host lavas preserve information on the style and dynamics of the mingling of magmas. Therefore, investigating the characteristics of enclaves promotes a more comprehensive understanding of the styles of mafic–silicic magma interactions, especially when considering if a discontinuity in magma composition can be stable in the magma body (e.g. Eichelberger *et al.*, 2000).

In this study, we document the morphological, chemical, and petrologic characteristics of two texturally distinct types of enclaves that exist in virtually all magmas erupted from Unzen for the past 500 kyr, sampled by flank drilling of the Unzen Scientific Drilling Project. The relationship of the enclaves to the volcanic sequence revealed by drilling will be discussed in a subsequent paper. We also present petrological and geochemical data from an andesite lava flow erupted from Mt. Unzen in 1663 because it is an unusually mafic lava composition not represented in the core stratigraphy. We begin with a brief overview of the geological setting of Unzen volcano, and then review our sampling and analytical methods. We follow with a description of the texturally distinct enclave types. We then propose a model for the generation of the enclave types.

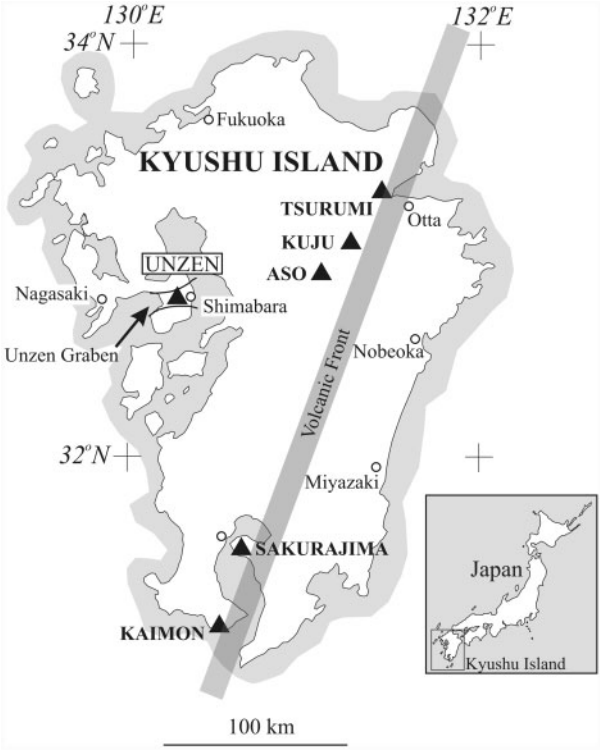

Fig. 1. Location map of Unzen volcano on Kyushu Island, Japan. The location of the Unzen Graben (after Hoshizumi *et al.*, 1999), the Japanese volcanic front (shaded), and other nearby active volcanic centers (▲), including Aso and Sakurajima, are also indicated.

GEOLOGICAL SETTING

Unzen volcano is situated in a volcano-tectonic depression known as the Unzen graben (Hoshizumi *et al.*, 1999), located ~70 km behind the volcanic front of SW Japan (Fig. 1). The volcanic products of Unzen volcano are lava domes, thick lava flows, and pyroclastic deposits that range in composition from andesite to dacite (~57–67 wt % SiO_2), with abundant large hornblende and plagioclase phenocrysts, and minor orthopyroxene, clinopyroxene, quartz, biotite, olivine, magnetite, ilmenite, and apatite.

Hoshizumi *et al.* (1999) and Uto *et al.* (2002) divided the eruptive history of the Unzen volcanic edifice into two main groups based on the age and composition of the erupted material, separated by an ~100 kyr repose period. Older Unzen is thought to be a complex of several different volcanic vents from which many lava domes, lava flows, and pyroclastic flows were erupted. K–Ar ages of Older Unzen deposits range from ~300 to 200 ka, although some deposits yield K–Ar ages of 500 ka (NEDO, 1988). Younger Unzen yielded K–Ar, ^{14}C, and fission-track ages of ~100 ka to present and is a collection of several different volcanic edifices, including Nodake, Mayuyama, satellite Mayuyama, and the youngest, Fugendake. Eruptive deposits from younger Unzen are typically lava domes, lava flows, and block-and-ash pyroclastic deposits.

MATERIALS AND ANALYTICAL TECHNIQUES

Three groups of samples are used in this study. The first group of samples consists of enclave-bearing dacite lava and dacite block-and-ash flow sequences intersected by the USDP-1 drill hole (752 m depth, Hoshizumi *et al.*, 2002) (Fig. 2). We selected these samples for study at the USDP core storage facility, located at the Geological Survey of Japan (GSJ) in Tsukuba City. The core was described, photographed and archived by the GSJ. Because the USDP core is an invaluable resource for future studies, only small pieces of enclave-bearing dacite lava were sampled by cutting the core into one-quarter, <5 cm longitudinal sections. The second group of samples consists of enclave-bearing dacite block and ash flow deposits from the 1991–1995 eruption. Samples of

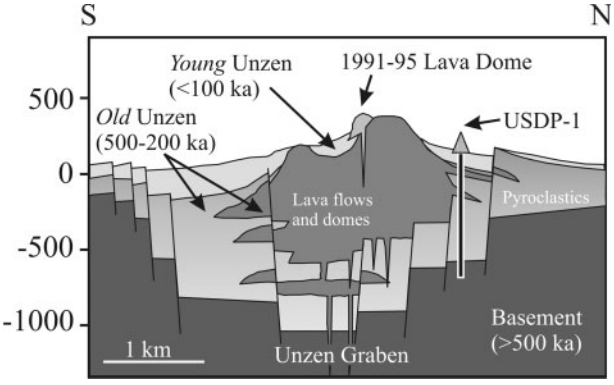

Fig. 2. Schematic cross-section of the eastern flank of Unzen volcano and Unzen graben with the location of the USDP-1 flank drill site and drill path. Modified after Hoshizumi *et al.* (2002).

the lavas from groups 1 and 2 are referred to as 'host' lavas in this study. The third sample group is from an andesite lava flow erupted from Unzen volcano in the year 1663.

The major element compositions of mineral and glass phases from the host lavas, enclaves and 1663 lava were analyzed using a Cameca SX-50 electron microprobe, equipped with four wavelength-dispersive spectrometers and one energy-dispersive spectrometer system, located at the University of Alaska Fairbanks. For all mineral phases, an accelerating voltage of 15 keV, a beam current of 10 nA, and a 2–3 μm focused electron beam were used. For all glass analyses, an accelerating voltage of 15 keV, a beam current of 10 nA, and an 8–10 μm defocused electron beam were used. To minimize sodium migration in glass analysis, sodium was counted in 2 s intervals for the first 10 s of each analysis, and the counts were regressed to determine the initial sodium content as outlined by Devine *et al.* (1995).

For whole-rock analysis, samples were first pulverized into fine powder with a ceramic flat plate grinder. Next, for each sample, 3 g of powdered sample were added to 9 g of lithium tetraborate (used as a flux), and 0·50 g of ammonium nitrate (used as an oxidizer). These materials were mixed, fused at 1000°C while continuously stirred in a platinum crucible in an oxidizing flame for at least 30 min, and then poured into disk-shaped platinum molds. These glass disks were then analyzed by X-ray fluorescence (XRF) and laser ablation inductively coupled plasma mass spectrometry (LA-ICP-MS) at Michigan State University. XRF data for major elements were processed using fundamental parameter reduction method (Criss, 1980) using XRFWIN software (Omni Instruments), and USGS and GSJ standards. Analytical precisions of major elements are <0·2 wt % and <3% for minor elements (www.glg.msu.edu/facilities/jb-1aXRF_ICP-MS-Stats.xls). XRF trace-element analyses were reduced by standard linear regression techniques. Precision for trace element acquisition by the XRF and ICP-MS systems is better than ±4% and ±10%, respectively (www.glg.msu.edu/facilities/jb-1aXRF_ICP-MS-Stats.xls). The standards span a wide range of silicate rock compositions, ensuring that unknown samples lie within the range of the standards.

RESULTS

Morphology and texture of enclaves

Enclaves are evenly distributed through the host lavas, ranging in size from ~0·25 cm to 30 cm in diameter. Enclaves are not observed in the 1663 andesite lava flow. The most noticeable distinction between the enclaves and the host lavas is the high crystal content (70–90 vol. %), smaller grain size and darker color of the enclaves compared with the host (Fig. 3). Two types of magmatic enclaves are texturally distinguished and are defined as Porphyritic and Equigranular. Porphyritic enclaves are spherical in shape, have well-developed crenulated, glassy margins, account for ~1 vol. % (visual estimate), and are usually larger than Equigranular enclaves, ranging in size from 5 to 30 cm in diameter. The texture of Porphyritic enclaves is characterized by abundant large plagioclase phenocrysts (Fig. 4) that exist in a groundmass composed of fine-grained, euhedral, elongate, acicular microphenocrysts of mostly plagioclase and hornblende crystals and interstitial glass. Microphenocrysts decrease in size with approach to the contact with the host lava, indicative of a chilled margin. Porphyritic enclaves also contain hornblende phenocrysts with rounded, reacted margins surrounded by clean rims, minor amounts of clinopyroxene, and trace amounts of olivine (Table 1).

Porphyritic enclaves contain a bimodal population of vesicles (Fig. 5). Large, spherical vesicles (500–1000 μm) occur most frequently in the center of enclaves, whereas smaller vesicles (50–100 μm) occur throughout the enclaves. Some of the larger vesicles appear to form through a process where smaller vesicles coalesce. A densely packed rim of plagioclase and hornblende microlites may surround large vesicles. Smaller vesicles are widespread, irregularly shaped, and exist in gaps between crystals (Fig. 5).

Equigranular enclaves are smaller than Porphyritic enclaves with an average size of ~2 cm and a range of 0·1–8 cm (Fig. 6), and may exist within Porphyritic enclaves but never the reverse. Equigranular enclaves are evenly distributed throughout lavas and are more abundant than Porphyritic enclaves, accounting for between 3 and 5 vol. % based on point counting. Equigranular enclaves become increasingly elliptical with increased size, with enclaves larger than 2 cm being characterized by length to width aspect ratios from ~1·5 to 3. Equigranular enclaves are coarser grained

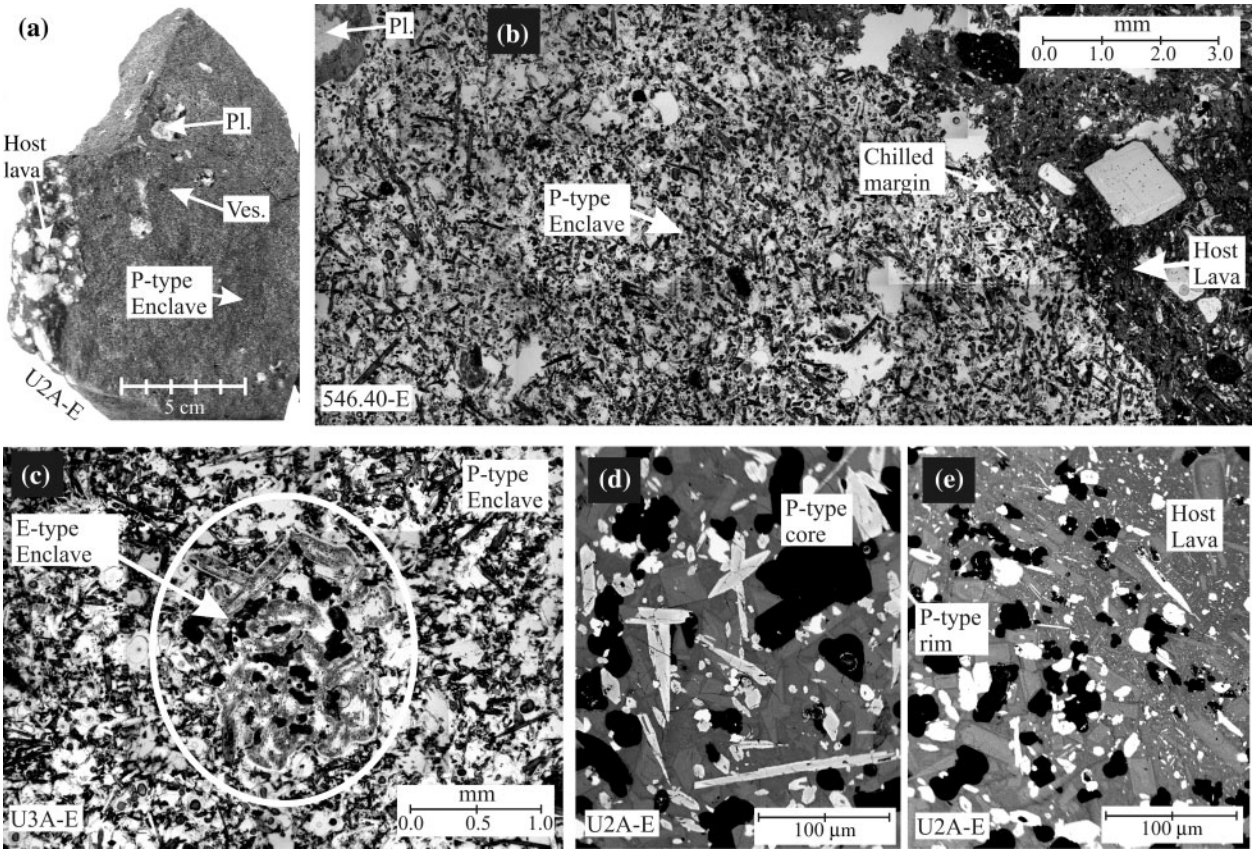

Fig. 3. Photomicrographs (a–c in plane-polarized light) and back-scattered electron images (d, e) showing the texture of Porphyritic (P-type) enclaves U2A-E, 546.40-E and U3A-E. P-type enclaves may contain Equigranular (E-type) enclaves (c). P-type enclaves are texturally characterized as being glass-rich with resorbed plagioclase phenocrysts in an acicular matrix. The cores of P-type enclaves are coarser grained and glass-poor (d) compared with enclave margins (e), indicative of chilling.

(100–500 μm) than Porphyritic enclaves and are composed of tabular and equant microphenocrysts of ~60–65 vol. % plagioclase, with less hornblende and orthopyroxene, trace amounts of clinopyroxene, and no olivine. Equigranular enclave microphenocrysts do not decrease in size with approach to the margin, nor are margins crenulated or chilled as in Porphyritic enclaves, but rather are defined by the protruding edges of microphenocrysts. Equigranular enclaves contain one population of 50–100 μm sized subrounded vesicles, and <10 vol. % glass (Fig. 5). No change in vesicle size or abundance appears to exist towards the center of these enclaves.

A few enclaves exhibit textures that appear intermediate between the Porphyritic and Equigranular end-members (Fig. 7). Intermediary enclaves contain a mineral assemblage of elongate plagioclase, hornblende, orthopyroxene, and Fe–Ti oxides. Intermediary enclaves also display porphyritic texture, containing phenocrystic plagioclase and hornblende with embayed or dissolved reaction rims, as in Porphyritic enclaves. Like Equigranular enclaves, however, intermediary enclaves are typically small in size (<2 cm). Intermediary enclaves are rare compared with the Porphyritic and Equigranular enclaves, occurring in only trace amounts in the host lava.

Whole-rock geochemistry

Unzen host lava (i.e. the lavas containing enclaves) samples are dacites and silicic andesites (Fig. 8, Table 2) (Miyashiro, 1974; Gill, 1981). Whole-rock host compositions range narrowly from 61·8 to 64·7 wt % SiO_2, from 2·3 to 3·0 wt % MgO, and from 2·2 to 2·6 wt % K_2O (Fig. 9). Whole-rock host lava Fe, Ca, Mg, Al, Mn, Sr, and Y concentrations generally decrease with increasing silica, whereas concentrations of K, Rb, Ba, and Zr are positively correlated with whole-rock silica abundance (Fig. 10).

Porphyritic enclaves range broadly from basalt through basaltic andesite to andesite (Fig. 8, Table 3), with 51·3–58·7 wt % SiO_2, 4·6–3·8 wt % MgO, and 1·2–1·8 wt % K_2O. Although whole-rock Fe, Ca, Mg, Mn, Al, Sr, and Y concentrations generally decrease with increasing silica

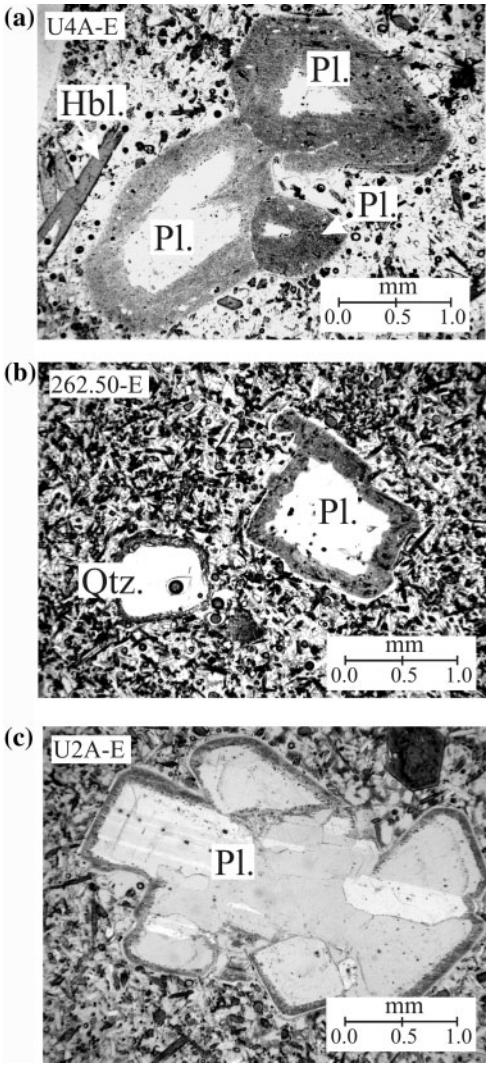

Fig. 4. Photomicrographs (in plane-polarized light) of resorbed plagioclase phenocrysts in Porphyritic enclaves U4A-E, 262.50-E, and U2A-E. Plagioclase phenocrysts that exist within Porphyritic enclaves commonly have cores of similar An range to host plagioclase phenocrysts and are invariably enclosed by a densely sieved resorption zone (dusty zone) of high An content. It should be noted that whereas plagioclase dusty zones vary in thickness from one enclave to another, the thicknesses among plagioclases within the same enclave are consistent. Porphyritic enclave plagioclase phenocrysts may also occur in clusters of 2–4 overlapping grains (U2A-E). In this case, the dusty zone occurs only where the cluster is in contact with the enclave matrix.

Table 1: Modal mineralogy of enclaves, host dacite and the 1663 lava

	Host dacite lava	Porphyritic enclave	Equigranular enclave	1663 lava
Glass	M	M	m	M
Plagioclase				
Oscillatory zoned phenocryst	M	m	A	M
Sieved core phenocryst	m	M	A	m
Resorbed rim phenocrysts	A	M	M	M
Reversely zoned microphenocryst	A	M	M	A
Hornblende				
Phenocryst	m	m	A	A
Resorbed phenocryst	m	m	A	A
Microphenocryst	A	M	m	A
Orthopyroxene	m	tr.	m	m
Clinopyroxene				
Phenocryst	tr.	m	A	m
Phenocryst with reaction rim	tr.	tr.	A	A
Olivine	tr.	tr.	A	tr.
Quartz				
Phenocryst	A	A	A	A
Resorbed phenocryst	tr.	tr.	A	tr.
Oxides	m	m	m	m
Vesicles				
Small (<150 μm)	m	m	m	tr.
Large (>250 μm)	tr.	m	A	A

M >20%; 20% > m > 1%; tr. <1%; A, absent.

and show broad correlation with host samples (Figs 9 and 10), only a few elements (e.g. Ca and Y) form tight arrays collinear with host dacites; others show considerable scatter. Equigranular enclaves narrowly range in composition from basaltic andesite to andesite (Figs 8–10, Table 4). Their evident scatter probably results from their small size (~2 cm average diameter) and coarse-grained texture. Equigranular enclaves overlap in composition with the most silicic Porphyritic enclaves.

The sample of the 1663 enclave-absent lava flow is medium-K calc-alkaline and plots on the boundary between basaltic andesite and andesite (Figs 8 and 9). The 1663 lava contains 57·1 wt % SiO_2, 4·5 wt % MgO, and 1·7 wt % K_2O, which is consistent with previous analyses performed by Nakada *et al.* (1999) (Table 5). The 1663 whole-rock compositions overlap the most silicic Porphyritic enclaves and the Equigranular enclaves in composition. Compared with the host lavas, the 1663 lava has Sr and Zr concentrations, but lower Rb and Ba, and higher Y concentrations (Fig. 10, Table 5). Concentrations of Rb and Y broadly plot on-trend between enclaves and host lava compositions in SiO_2 variation diagrams, whereas Sr does not.

Glass and phenocryst compositions

Lavas analyzed in this study are generally similar to those described previously by Hoshizumi *et al.* (1999) and Nakada & Motomura (1999). Host lava samples are

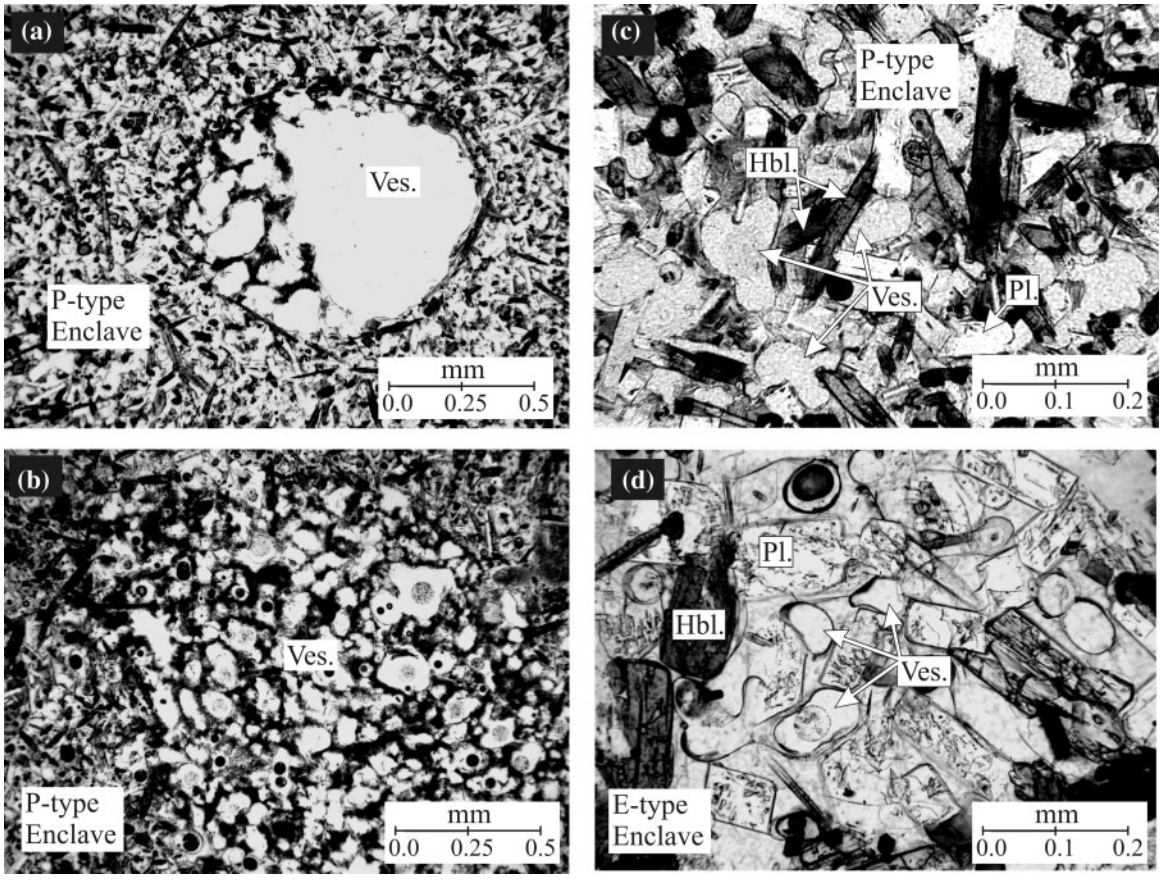

Fig. 5. Photomicrographs of vesicles in Porphyritic (a, b) and Equigranular (c, d) enclaves (in plane-polarized light). Porphyritic enclaves contain large, spherical vesicles (500–1000 μm) that occur most frequently in the center of enclaves. Both enclave types contain abundant smaller vesicles ranging in diameter from 50 to 100 μm that occur throughout the enclaves. Some large vesicles in Porphyritic enclaves appear to be the result of smaller vesicles coalescing (a, b).

crystal-rich, averaging between 30 and 40% crystals by volume, with large plagioclase and hornblende as the dominant phenocryst phases. Other minerals such as clinopyroxene, orthopyroxene, quartz, magnetite, ilmenite, olivine (with opx rims), biotite, and apatite may also be present in varying amounts. In addition to individual phenocryst phases, glomeroporphyritic aggregates of calcic plagioclase, orthopyroxene, clinopyroxene, and Fe–Ti oxide crystals are observed throughout the lavas.

The 1663 lava contains between 20 and 25 vol. % phenocrysts, comprising plagioclase (15–20 vol. %), clinopyroxene (3–4 vol. %), and orthopyroxene (1–2 vol. %). The remaining phenocryst phases are magnetite, ilmenite, quartz and pseudomorphs of hornblende. Quartz and hornblende are considered to be unstable, as indicated by reaction rims of clinopyroxene and plagioclase that always enclose quartz, and hornblendes are almost completely replaced with Fe–Ti oxides, plagioclase, and clinopyroxene.

Both types of enclaves are dominated by euhedral plagioclase and hornblende, with lesser amounts of orthopyroxene, magnetite, ilmenite, glass, and vesicles. In addition, Porphyritic enclaves contain clinopyroxene, olivine, quartz (always embayed or reacted), and biotite (always reacted) exclusively, whereas Equigranular enclaves contain trace amounts of apatite. Mineral and glass compositions are given in Tables 6–10, and specific characteristics of each phase are described below.

Glass

Glass forms 60–70 vol. % of the host lava samples and the 1663 lava sample. Glass accounts for 15–20 vol. % in Porphyritic enclaves (>20 vol. % at the enclave edge), and ~10 vol. % in Equigranular enclaves. Porphyritic enclave glasses overlap with 1663 lava glass with respect to Na_2O, K_2O, and CaO, but not Fe_2O_3, Al_2O_3, or TiO_2 (Fig. 11). Equigranular glass compositions have an identical range compared with host lava glasses (Fig. 11, Table 6). In addition, enclave glasses are clear whereas host lava matrix glasses are charged with microlites.

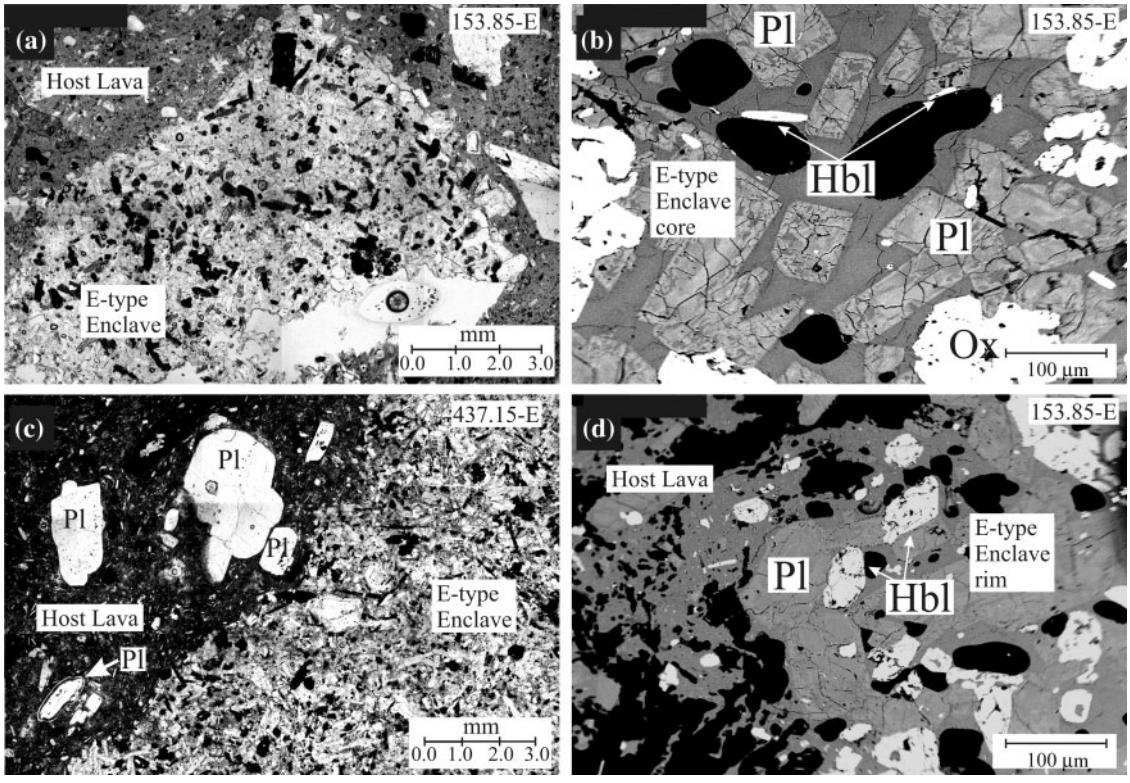

Fig. 6. Photomicrographs (a, c in plane-polarized light) and back-scattered electron images (b, d) showing the texture of Equigranular (E-type) enclaves 153.85-E and 437.15-E. Phenocryst phases: Pl, plagioclase; Hbl, hornblende; Ox, Fe–Ti oxide.

Plagioclase

Plagioclase is the most abundant phenocryst phase in the Unzen lavas. Phenocrystic plagioclases make up 15–25 vol. % of host lavas, and are divided into three main populations based on texture and composition (Fig. 12). The most common population of plagioclase is represented by large oscillatory-zoned euhedral grains (0·25–1 cm in length) with core compositions of $An_{45–65}$ and medial zones ranging from An_{50} to An_{70} (Fig. 12a).

A second population is composed of grains with coarsely sieved cores with a composition that ranges from An_{60} to An_{85} (Fig. 12b). The coarsely sieved texture results from the presence of abundant, interconnecting, 10–20 μm inclusions of pyroxene, hornblende and glass (melt) that appear to pervade the crystals' interior. Plagioclases with resorption (dusty) zones that surround the interiors of oscillatory-zoned plagioclase phenocrysts, but rarely coarsely sieved plagioclase, characterize the third population (Fig. 12c). Resorption zones are composed of a network of profuse micron-sized glass inclusions amid 5–15 μm plagioclase regions of high-An composition ($An_{70–90}$), abruptly more calcic than the interior region of the phenocrysts. Resorption zones cut across oscillatory zoning patterns and have a wide range in thickness from 30 to 400 μm. The texture and composition of these resorption zones strongly resemble those replicated by Nakamura & Shimakita (1998) in heating experiments. Clear rims enclose virtually all plagioclase grains found in the host lavas. Rims are often defined by euhedral to subhedral crystal faces and exhibit strong normal zoning patterns across a thickness of 0·01–0·08 mm. Rim compositions range from An_{80} to An_{65}.

Plagioclase is also the most common phenocryst phase in the 1663 lava flow, accounting for 15–20 vol. %. The 1663 lava plagioclases (Fig. 13a and b) are euhedral to subhedral grains (0·05–0·6 cm in length) with a wide range in core compositions ($An_{45–75}$). The most common type has either normally or oscillatory zoned cores ranging from An_{70} to An_{50}, and is oscillatory zoned from the core towards the rim, where anorthite content ranges from An_{50} to An_{70}. A second population of plagioclases in the 1663 lava contains coarsely sieved interiors with core compositions ranging from An_{70} to An_{85}. All plagioclases observed in the 1663 lava flow are surrounded by resorption zones with a high An content ($An_{75–90}$). Resorption zones in plagioclases from the 1663 lava have a narrower range of thickness (30–90 μm) compared with that of other host lavas (30–400 μm), and are characterized by a tightly packed network of fine-grained (~1 μm) glass inclusions. Enclosing the resorption zones are thin (10–50 μm), clear rims

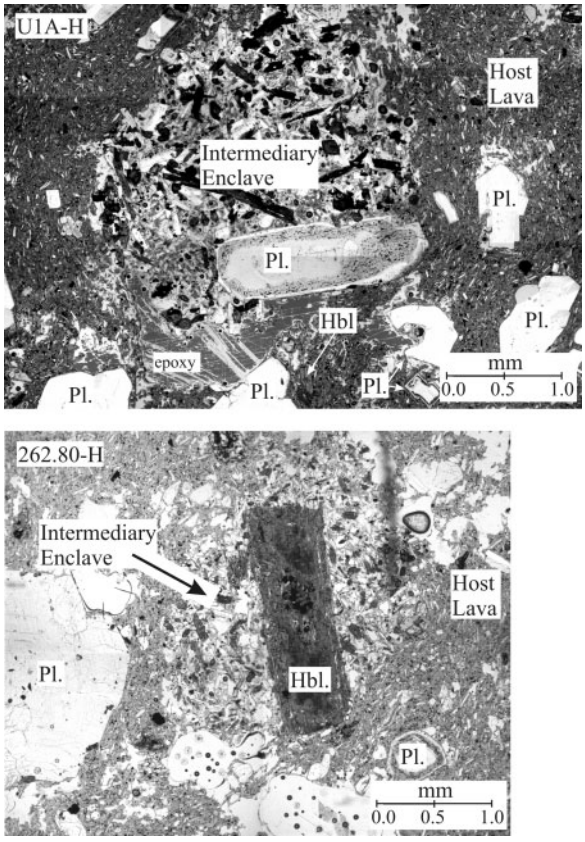

Fig. 7. Photomicrographs (in plane-polarized light) showing the texture of enclaves that are intermediate in texture with respect to either end-member from samples U1A-H and 262.80-H. Phenocryst phases: Pl, plagioclase; Hbl, hornblende. Portions of thin section where epoxy is present are indicated.

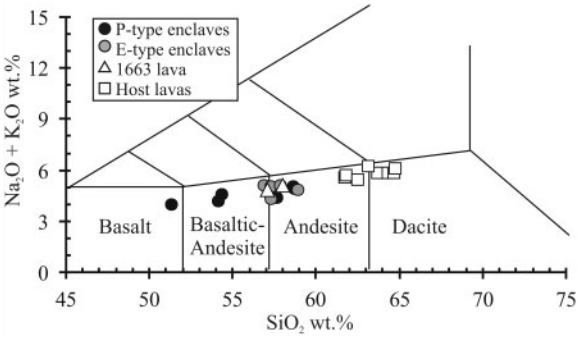

Fig. 8. IUGS chemical classification scheme for volcanic rocks (Le Bas *et al.*, 1986) for host lava (□), Porphyritic enclaves (●), Equigranular enclaves (●) and 1663 lava (△). It should be noted that E-type enclaves are narrowly distributed in composition with respect to silica and overlie the most silicic P-type enclave composition. E-type enclaves are also equivalent to the 1663 lava in bulk composition.

($An_{70–85}$) with euhedral edges where in contact with the glass. Many 1663 plagioclase grains appear broken, as indicated by their cracked morphology and truncated oscillatory zoning patterns. It is unlikely, however, that these crystals were fractured during ascent or emplacement because they too are surrounded by resorption zones of high An content ($An_{75–85}$) and finally enclosed by thin, clear, high-An rims ($An_{85–75}$).

Phenocrystic plagioclase is a diagnostic phase in Porphyritic enclaves, accounting for between 3 and 5 vol. % (Figs 4 and 13). The phenocrysts range in size from 0·2 to 8 mm in diameter, and have cores, which are most commonly oscillatory zoned, of similar An range to those plagioclase types in host lava plagioclase ($An_{50–60}$). These cores are invariably enclosed by resorption zones of high An content ($\sim An_{80}$). Resorption zones vary in thickness from one enclave to another (30–500 μm), but are consistent among plagioclases within the same enclave. Porphyritic enclave phenocrystic plagioclases contain a thin clear rim (<30 μm) that matches the rim composition of both the coexisting microphenocryst plagioclase ($An_{60–40}$) and the plagioclase found in the host lavas (Fig. 13). Phenocrystic plagioclase found in Porphyritic enclaves may also occur in clusters of 2–4 overlapping grains (Figs 4 and 13c). In this case, resorption zones continue across grain boundaries following the contact with the enclave matrix. Coarsely sieved plagioclases ($An_{72–85}$ cores) rarely occur as phenocrysts in enclaves, and when they do, they typically do not contain resorption zones.

Plagioclase microphenocrysts make up 50–55 vol. % of Porphyritic enclaves and are euhedral, elongate grains (50–200 μm long, 20–40 μm wide) compared with the larger, tabular, and more equant microphenocryst plagioclase found in Equigranular enclaves (100–500 μm long, 80–300 μm wide). Plagioclase microphenocrysts make up 60–65 vol. % of Equigranular enclaves. Both Porphyritic and Equigranular enclave microphenocryst plagioclase have large normal compositional gradients from core to rim (Fig. 14). Porphyritic enclave microphenocryst plagioclase cores range between An_{80} and An_{90}, whereas Equigranular plagioclase cores range from An_{75} to An_{85}; plagioclases from both types have rim compositions of $An_{50–60}$. Rim compositions of microphenocryst plagioclase overlap the range of host lava plagioclase rims. Finally, although the plagioclase core and rim compositions from Porphyritic and Equigranular enclaves are similar, the nature of the zoning from one type to another is distinct. Whereas elongate Porphyritic microphenocrysts are steeply normally zoned (Fig. 14a), tabular Equigranular microphenocrysts display a more gradual normal zonation towards the rim (Fig. 14b).

Hornblende

Hornblende phenocrysts account for between 5 and 8 vol. % of the host lavas, and occur as either dark brown, medium-grained (1–5 mm), equant phenocrysts,

Table 2: Whole-rock compositions of host lava samples

Sample:	U1A-H	103.80-H	153.85-H	198.90-H	262.80-H	390.00-H	437.15-H	546.45-H	602.80-H
Depth (m):	0·00	103·80	153·85	198·90	262·80	390·00	437·15	546·45	602·80
wt %									
SiO_2	63·95	61·75	63·69	64·30	61·78	64·69	62·50	63·12	64·72
TiO_2	0·67	0·73	0·69	0·70	0·78	0·71	0·78	0·70	0·79
Al_2O_3	16·15	17·04	15·68	15·96	16·49	15·65	16·30	15·84	15·58
Fe_2O_3*	4·98	5·44	5·10	4·78	5·58	5·24	6·04	5·01	5·31
MnO	0·10	0·11	0·10	0·10	0·11	0·11	0·12	0·10	0·09
MgO	2·65	2·67	2·62	2·37	2·99	2·29	2·71	2·43	2·29
CaO	5·23	5·83	5·22	4·98	5·71	4·89	5·68	4·61	4·59
Na_2O	3·57	3·39	3·26	3·49	3·38	3·22	3·19	3·74	3·48
K_2O	2·24	2·16	2·57	2·38	2·31	2·59	2·26	2·49	2·61
P_2O_5	0·16	0·16	0·16	0·16	0·19	0·17	0·17	0·17	0·21
Total	99·70	99·28	99·09	99·22	99·32	99·56	99·75	97·91	99·67
ppm									
Ni	29	23	25	25	26	17	14	69	37
Cu	27	27	24	28	15	16	10	26	21
Zn	54	55	49	52	55	54	62	55	50
Rb	75	63	82	77	70	81	68	87	85
Zr	148	159	163	165	176	173	147	164	182
Sr	333	408	356	372	376	364	431	371	346
Y	14·85	17·42	15·18	16·16	19·72	16·52	18·98	15·67	17·65
Nb	19·09	18·00	25·42	26·56	24·80	22·22	16·66	25·86	32·25
Ba	458·91	474·38	515·05	529·71	485·32	534·94	449·53	571·19	530·53
La	22·03	22·70	22·95	23·55	26·10	23·67	22·01	24·56	26·37
Ce	44·30	41·05	45·69	47·79	46·79	46·27	38·91	49·02	50·99
Pr	4·62	4·70	4·90	5·27	5·68	5·36	4·86	5·33	5·99
Nd	16·01	17·08	17·20	18·69	20·98	18·68	18·79	18·47	21·15
Sm	3·09	3·45	3·28	3·67	4·13	3·56	3·84	3·47	4·10
Eu	1·02	1·10	1·00	1·07	1·18	1·07	1·14	1·07	1·10
Gd	2·60	2·80	2·72	2·87	3·39	2·93	3·22	2·80	3·27
Tb	0·41	0·46	0·41	0·45	0·55	0·46	0·52	0·43	0·52
Dy	2·29	2·71	2·36	2·52	3·12	2·66	2·96	2·49	2·95
Ho	0·46	0·55	0·46	0·49	0·62	0·53	0·58	0·49	0·58
Er	1·31	1·60	1·37	1·45	1·72	1·53	1·72	1·37	1·66
Yb	1·23	1·60	1·26	1·31	1·75	1·49	1·72	1·24	1·57
Lu	0·20	0·24	0·21	0·22	0·27	0·24	0·28	0·22	0·25
Hf	2·46	2·95	2·69	2·76	3·39	3·21	3·08	2·81	3·40
Ta	2·87	3·87	6·79	7·77	7·74	6·20	4·26	5·61	10·87
Pb	13·48	10·37	14·72	14·82	9·70	12·93	9·38	16·36	13·23
Th	7·18	7·27	7·19	7·11	7·45	8·17	7·35	8·12	8·68
U	2·66	1·84	2·67	2·62	1·83	2·44	1·81	2·97	2·60
Cr	45·20	47·20	57·80	45·80	45·40	32·70	35·40	63·20	21·00

Major oxides and Ni–Sr were determined by XRF, the others by LA-ICP-MS. U1A-H is from the 1991–1995 eruption sample group; the other samples are from Unzen Scientific Drilling Project USDP-1 drill core.
*Total Fe calculated as Fe_2O_3.

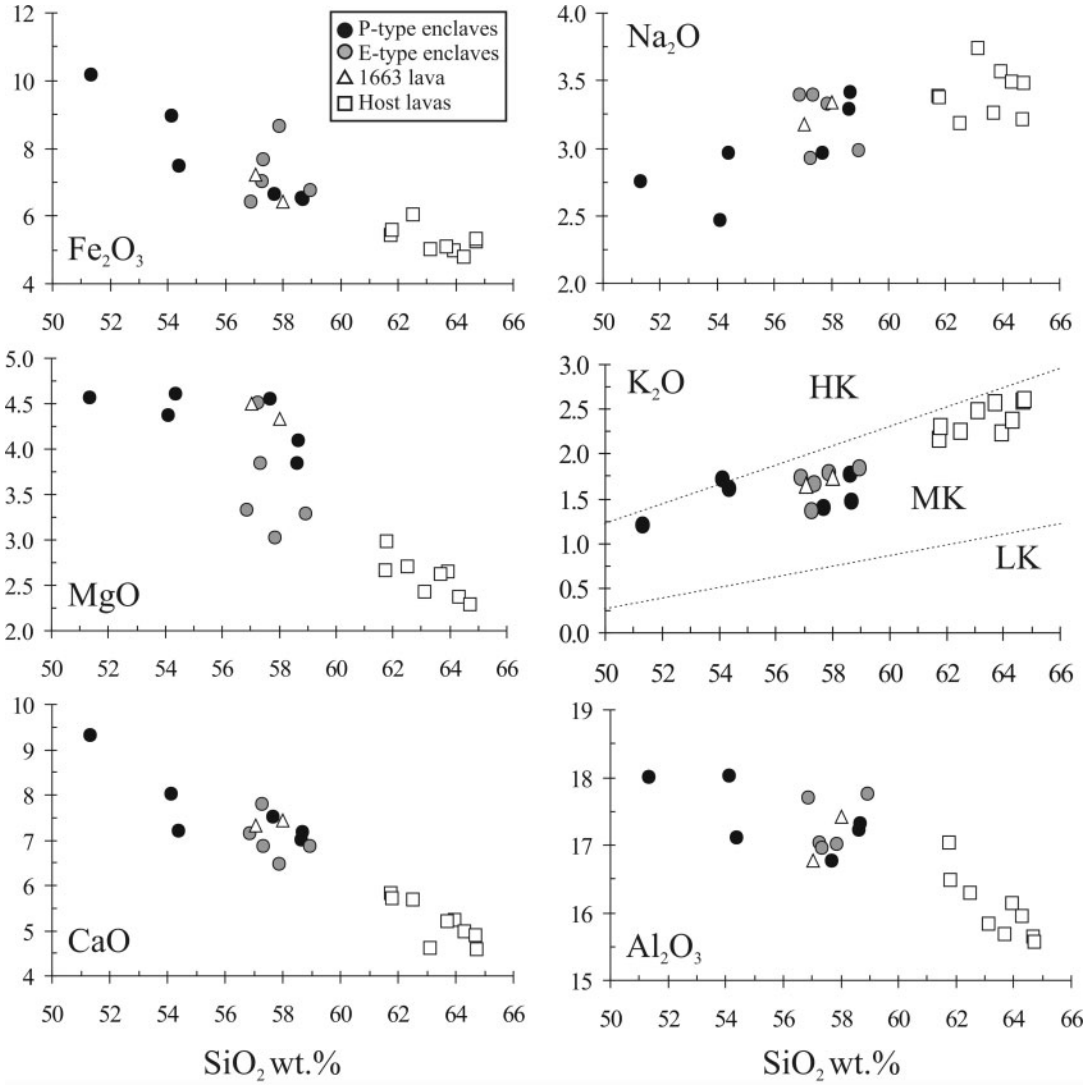

Fig. 9. Major oxide–SiO_2 variation diagrams for host lava, Porphyritic enclaves, Equigranular enclaves, and 1663 lava. High-K, Medium-K, and Low-K trends from Le Maitre *et al.* (1989).

or as large (5–8 mm), equant phenocrysts with rounded or embayed rims. A thin rim of pyroxene, plagioclase, and Fe–Ti oxides may enclose phenocrystic hornblendes, whereas other grains appear to have no rims, even when separated from each other by less than a few millimeters. Hornblende phenocrysts commonly have inclusions of plagioclase, biotite, clinopyroxene, glass, and Fe–Ti oxides. Medium-grained hornblendes typically do not have rounded or embayed rims, nor do they contain biotite or quartz inclusions.

Hornblende microphenocrysts are the dominant mafic mineral phase in the enclaves, and account for 20–25 vol. % in Porphyritic enclaves, and 15–25 vol. % in Equigranular enclaves. Hornblendes found in Porphyritic enclaves are texturally distinct from hornblendes of the host lavas and Equigranular enclaves, in that they are smaller, highly elongate, compositionally zoned, and typically have hollow cores. Equigranular enclave hornblendes are larger, prismatic, and typically compositionally unzoned.

There is a large variation in hornblende composition found in enclaves and host lava. Cores of hornblendes in Porphyritic enclaves contain about twice the Al_2O_3, TiO_2, and Na_2O as the rim, and rim compositions of Porphyritic enclave hornblende approach the composition of Equigranular enclave and host lava. Furthermore, hornblende cores from Porphyritic enclaves have elevated $Al^{(IV)}$ and (Na + K) compared with the host lava hornblende cores, although rim compositions may overlap (Fig. 15). In contrast, Equigranular enclaves have hornblende core and rim $Al^{(IV)}$ and (Na + K) compositions similar to those in host lavas.

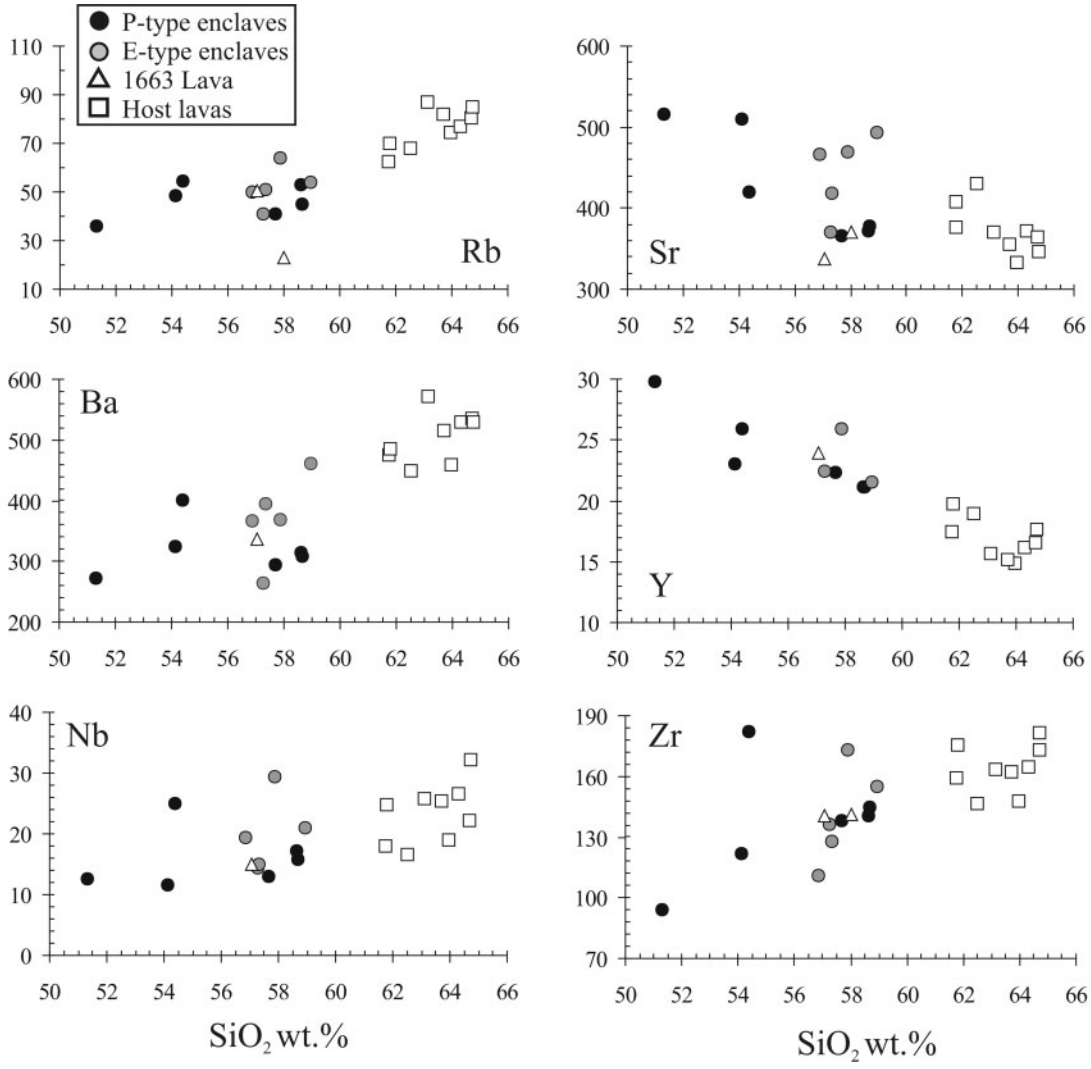

Fig. 10. Trace element (in parts per million, ppm) vs SiO_2 variation diagrams for host lava, Porphyritic enclaves, Equigranular enclaves, and 1663 lava.

Hornblende in 1663 lava occurs as relics, having been almost completely replaced with Fe–Ti oxides, plagioclase, and clinopyroxene. Hornblende relics account for between 2 and 3 vol. % of the 1663 lava, and range in size from 5 to 8 mm. Hornblende is also observed enclosing some olivine phenocrysts as reaction rims.

Pyroxenes

Pyroxenes account for <3 vol. % of the host lavas and 2–5 vol. % in the enclaves. Orthopyroxene and clinopyroxene are commonly found in glomeroporphyritic aggregates with calcic plagioclase and Fe–Ti oxides that occur in host lavas and Porphyritic enclaves. These clinopyroxenes are invariably rimmed by orthopyroxene and plagioclase where in contact with the host groundmass. When pyroxenes exist as single crystals in the host lavas, clinopyroxenes are subhedral to anhedral, and many have resorbed rims, whereas orthopyroxenes are euhedral to subhedral. Orthopyroxene is found in both types of enclaves, and is typically euhedral in Porphyritic enclaves and subhedral in Equigranular enclaves. In contrast, clinopyroxene is found in all Porphyritic enclaves, but only a single grain was found in Equigranular enclaves. Orthopyroxenes of Porphyritic enclaves have a wide range in composition (Fig. 16) compared with those in Equigranular enclaves or host lavas. Clinopyroxenes of Porphyritic enclaves are tightly clustered around a composition of $Wo_{45}En_{35}Fs_{10}$, and are not systematically zoned.

Pyroxenes account for 4–7 vol. % of the 1663 lava, second in abundance to plagioclase. They most

Table 3: Whole-rock compositions of Porphyritic enclaves

Sample:	U2A-E	U3A-E	U4A-E	262.50-E	435.20-E	546.40-E
Depth (m):	0·00	0·00	0·00	262·50	435·20	546·40
wt %						
SiO_2	58·67	57·68	58·63	54·37	54·11	51·32
TiO_2	0·87	0·86	0·88	0·96	0·96	1·27
Al_2O_3	17·33	16·78	17·22	17·11	18·03	18·01
Fe_2O_3*	6·51	6·65	6·55	7·48	8·97	10·17
MnO	0·12	0·13	0·12	0·14	0·16	0·18
MgO	4·10	4·56	3·85	4·61	4·37	4·57
CaO	7·18	7·53	7·02	7·22	8·03	9·33
Na_2O	3·42	2·97	3·29	2·97	2·47	2·76
K_2O	1·47	1·41	1·78	1·62	1·73	1·21
P_2O_5	0·17	0·17	0·19	0·21	0·18	0·17
Total	99·84	98·74	99·53	96·69	99·01	98·99
ppm						
Ni	40	47	40	172	16	16
Cu	43	52	55	41	4	21
Zn	62	56	60	62	77	69
Rb	45	41	53	55	48	36
Zr	145	138	141	182	122	94
Sr	378	366	373	420	511	516
Y	21·16	22·37	21·17	25·96	23·04	29·84
Nb	15·74	13·06	17·12	25·02	11·59	12·53
Ba	308·82	294·20	315·57	401·27	324·35	272·88
La	18·91	19·24	19·66	27·51	16·31	12·64
Ce	34·25	35·41	34·95	47·20	30·48	23·17
Pr	4·36	4·60	4·42	6·10	4·44	3·61
Nd	17·37	18·52	17·61	23·95	19·13	25·20
Sm	3·76	4·15	3·89	4·99	4·37	4·39
Eu	1·11	1·19	1·12	1·36	1·32	1·35
Gd	3·35	3·64	3·48	4·34	3·81	4·36
Tb	0·55	0·59	0·57	0·70	0·62	0·75
Dy	3·21	3·54	3·27	4·15	3·67	4·79
Ho	0·66	0·72	0·66	0·83	0·74	0·98
Er	1·92	2·07	1·91	2·35	2·10	2·80
Yb	1·94	2·05	1·95	2·28	2·10	2·67
Lu	0·29	0·32	0·30	0·35	0·33	0·41
Hf	2·95	3·01	2·90	3·84	2·73	2·38
Ta	4·40	2·37	5·77	7·93	4·28	5·81
Pb	6·57	6·87	7·22	7·03	8·43	3·49
Th	4·96	4·95	5·22	6·47	3·39	2·84
U	1·18	1·11	1·20	1·20	0·72	0·55
Cr	65·20	72·20	45·10	63·50	33·00	37·80

Major oxides and Ni–Sr were determined by XRF, the others by LA-ICP-MS. U2A-E, U3A-E and U4A-E are from the 1991–1995 eruption sample group; 262.50-E, 546.40-E and 435.20-E are from Unzen Scientific Drilling Project USDP-1 drill core.
*Total Fe calculated as Fe_2O_3.

Table 4: Whole-rock compositions of Equigranular enclaves

Sample:	U5A-E	153.85-E	199.10-E	390.00-E	602.80-E
Depth (m):	0·0	153·9	199·1	390·0	602·8
wt %					
SiO_2	57·26	56·87	57·33	58·94	57·87
TiO_2	0·90	1·01	1·02	0·91	1·35
Al_2O_3	17·04	17·71	16·97	17·76	17·02
Fe_2O_3*	7·02	6·44	7·66	6·77	8·65
MnO	0·12	0·13	0·16	0·12	0·12
MgO	4·52	3·33	3·85	3·29	3·03
CaO	7·79	7·16	6·88	6·86	6·48
Na_2O	2·93	3·40	3·40	2·99	3·33
K_2O	1·37	1·74	1·67	1·85	1·80
P_2O_5	0·17	0·38	0·13	0·18	0·31
Total	99·12	98·17	99·07	99·67	99·96
ppm					
Ni	47	34	30	19	32
Cu	33	127	92	17	20
Zn	59	63	76	60	73
Rb	41	50	51	54	64
Zr	136	111	128	155	173
Sr	371	467	418	493	470
Y	22·44	33·28	30·11	21·53	25·88
Nb	14·43	19·34	15·06	20·92	29·45
Ba	265·05	366·93	395·62	460·65	368·08
La	17·92	33·30	24·07	23·55	26·62
Ce	31·93	65·08	47·23	41·89	46·62
Pr	4·34	8·00	6·04	5·60	6·32
Nd	17·72	32·12	24·46	22·43	25·37
Sm	3·94	6·79	5·31	4·90	5·38
Eu	1·14	1·57	1·44	1·43	1·33
Gd	3·56	6·20	4·98	3·99	4·49
Tb	0·58	0·96	0·81	0·62	0·73
Dy	3·50	5·90	5·18	3·41	4·50
Ho	0·71	1·13	0·99	0·67	0·90
Er	2·11	3·52	3·10	1·92	2·50
Yb	2·13	3·32	3·11	1·88	2·42
Lu	0·32	0·50	0·49	0·29	0·36
Hf	2·99	3·28	4·10	3·34	3·71
Ta	4·69	1·52	1·27	10·60	9·87
Pb	5·90	8·94	8·04	7·41	7·23
Th	4·61	8·47	7·97	6·13	6·83
U	0·98	1·27	1·12	1·23	1·46
Cr	64·80	75·80	44·30	38·50	0·10

Major oxides and Ni–Sr were determined by XRF, the others by LA-ICP-MS. U5A-E is from the 1991–1995 eruption sample group; the other samples are from the Unzen Scientific Drilling Project USDP-1 drill core sample group.
*Total Fe calculated as Fe_2O_3.

Table 5: Whole-rock compositions of the 1663 lava

Sample:	UZN-1663	Nakada *et al.* (1999)
wt %		
SiO_2	57·05	58·01
TiO_2	1·01	0·94
Al_2O_3	16·77	17·42
Fe_2O_3*	7·22	6·41
MnO	0·14	0·13
MgO	4·50	4·34
CaO	7·33	7·45
Na_2O	3·18	3·34
K_2O	1·65	1·74
P_2O_5	0·22	0·21
Total	99·07	99·99
ppm		
Ni	—	—
Cu	—	—
Zn	—	—
Rb	51	23
Zr	141	137
Sr	338	371
Y	23·92	—
Nb	14·77	—
Ba	336·55	—
La	18·55	—
Ce	36·73	—
Pr	4·43	—
Nd	17·57	—
Sm	3·65	—
Eu	1·15	—
Gd	3·82	—
Tb	0·64	—
Dy	3·45	—
Ho	0·81	—
Er	2·30	—
Yb	2·13	—
Lu	0·34	—
Hf	3·07	—
Ta	0·91	—
Pb	5·95	—
Th	5·95	—
U	0·91	—
Cr	57·88	—

Major oxides and Ni–Sr were determined by XRF, the others by LA-ICP-MS. UZN-1663 is a 1663 lava sample.
*Total Fe calculated as Fe_2O_3.

commonly occur as isolated phenocrysts rather than in glomeroporphyritic aggregates as in the host lava samples. Clinopyroxene phenocrysts are equant and 20–200 μm in length. They are euhedral to subhedral with an average composition of $Wo_{42}En_{40}Fs_{18}$, and are rarely enclosed by a reaction rim. Orthopyroxene phenocrysts are predominantly subhedral and range between 20 and 100 μm in size, and have an average composition of $Wo_5En_{58}Fs_{37}$. Orthopyroxene also encloses most olivine phenocrysts as reaction rims.

Fe–Ti oxides

Magnetite and ilmenite are present in all the host lavas, in the 1663 lava, and in the majority of enclave samples. Together, magnetite and ilmenite account for between 1 and 2 vol. % of the host lavas and the 1663 lava, and slightly more in enclaves (1–3 vol. %). Magnetite occurs as small subhedral, or irregularly shaped phenocrysts in the host lavas and the 1663 andesite, but is typically euhedral in enclaves. Many host lavas and Equigranular enclaves contain magnetite grains with ilmenite exsolution lamellae, probably resulting from slow cooling in the interior of lava flows and domes. Ilmenite occurs as small subhedral crystals in the host lavas and enclaves, but as anhedral or irregularly shaped crystals in the 1663 andesite. Ilmenite is less abundant than magnetite in all samples, occurring in only trace amounts (<1 vol. %).

Magnetite and ilmenite disequilibrium textures, such as irregular crystal faces in 1663 lava and exsolution textures in host lavas and enclaves, are widespread, thereby complicating efforts to make estimates of pre-eruptive temperatures. All such estimates presented in this study are limited to analyses of touching magnetite and ilmenite grains, with euhedral crystal faces, where the pair compositions are potentially in equilibrium, based on the model of Bacon & Hirschmann (1988). All geothermometry in this study employs the mineral recalculation scheme of Stormer (1983) and the algorithm of Andersen & Lindsley (1988).

Magnetite–ilmenite pairs from host lava samples are compositionally zoned (Table 10), yielding a temperature range of 725–810°C from pair cores and 820–830°C for pair rims, with an oxygen fugacity of NNO + 1·5 (where NNO is the nickel–nickel oxide buffer). These estimates are similar to those obtained in earlier studies (Venezky & Rutherford, 1999). Magnetite–ilmenite pairs from Porphyritic enclaves are either unzoned or are surrounded by a thin rim (<10 μm) of differing composition. Porphyritic enclave pairs yield temperatures between 955 and 1040°C (only two samples yield temperatures >1000°C) from pair cores and an oxygen fugacity of between NNO + 0·5 and NNO + 0·25. Where present, thin rims yield a temperature range of 825–895°C ($n = 2$), and an oxygen fugacity of approximately NNO – 1·0. It seems likely, however, that most Porphyritic enclave magnetite–ilmenite pairs did not have enough time to fully re-equilibrate with the host before ascent and subsequent quenching, and thus these temperature estimates

Table 6: Electron microprobe (oxides in wt %) analyses of glass

Sample	*n*	SiO_2	Al_2O_3	TiO_2	Fe_2O_3	MgO	CaO	Na_2O	K_2O	Cl	Total
153.85-H (host lava)	10	73·67	12·29	0·16	1·33	0·17	0·81	2·79	5·17	0·10	96·49
Volatile-free		76·35	12·74	0·17	1·38	0·18	0·84	2·89	5·36	0·10	100·00
199.10-H (host lava)	10	73·67	11·93	0·35	1·73	0·45	0·68	2·31	5·72	0·03	96·87
Volatile-free		76·05	12·32	0·36	1·79	0·46	0·70	2·38	5·90	0·03	100·00
390.00-H (host lava)	10	74·66	11·47	0·21	1·09	0·12	0·72	2·74	4·98	0·10	96·09
Volatile-free		77·70	11·94	0·22	1·13	0·12	0·75	2·85	5·18	0·10	100·00
435.20-H (host lava)	10	74·35	12·71	0·25	0·96	0·11	1·24	2·82	5·09	0·07	97·60
Volatile-free		76·18	13·02	0·26	0·98	0·11	1·27	2·89	5·22	0·07	100·00
546.45-H (host lava)	10	74·71	12·68	0·16	0·86	0·18	0·90	2·96	5·37	0·04	97·86
Volatile-free		76·34	12·96	0·16	0·88	0·18	0·92	3·02	5·49	0·04	100·00
602.80-H (host lava)	10	75·62	13·19	0·22	0·73	0·07	1·36	3·26	4·69	0·02	99·16
Volatile-free		76·26	13·30	0·22	0·74	0·07	1·37	3·29	4·73	0·02	100·00
U5A-H (host lava)	10	76·52	12·81	0·38	1·36	0·16	1·12	3·32	4·36	0·05	100·08
Volatile-free		76·46	12·80	0·38	1·36	0·16	1·12	3·32	4·36	0·05	100·00
262.5-E (P-type)	10	71·13	13·55	0·59	1·85	0·16	1·12	4·97	3·34	0·06	96·76
Volatile-free		73·51	14·00	0·61	1·91	0·17	1·16	5·14	3·45	0·06	100·00
435.20-E (P-type)	10	71·38	13·56	0·31	1·11	0·07	0·49	6·91	2·78	0·05	96·74
Volatile-free		73·79	14·02	0·32	1·15	0·07	0·51	7·14	2·87	0·05	100·00
546.25-E (P-type)	10	73·68	12·03	0·16	0·71	0·09	0·51	6·27	2·41	0·03	95·89
Volatile-free		76·84	12·55	0·17	0·74	0·09	0·53	6·54	2·51	0·03	100·00
U1A-E (P-type)	10	72·62	14·24	0·35	1·91	0·13	1·09	5·31	3·74	0·09	99·48
Volatile-free		73·00	14·31	0·35	1·92	0·13	1·10	5·34	3·76	0·09	100·00
U2A-E (P-type)	10	74·09	13·13	0·55	1·38	0·08	0·53	6·37	3·05	0·05	99·23
Volatile-free		74·66	13·23	0·55	1·39	0·08	0·53	6·42	3·07	0·05	100·00
U4A-E (P-type)	10	73·55	13·56	0·32	1·84	0·24	1·23	4·31	3·55	0·07	98·67
Volatile-free		74·54	13·74	0·32	1·86	0·24	1·25	4·37	3·60	0·07	100·00
153.85-E (E-type)	10	73·67	12·29	0·16	1·33	0·17	0·81	5·17	2·79	0·10	96·49
Volatile-free		76·35	12·74	0·17	1·38	0·18	0·84	5·36	2·89	0·10	100·00
199.10-E (E-type)	10	73·00	12·10	0·10	0·70	0·20	0·60	2·20	4·90	0·10	93·90
Volatile-free		77·74	12·89	0·11	0·75	0·21	0·64	2·34	5·22	0·11	100·00
390.00-E (E-type)	10	74·66	11·47	0·21	1·09	0·12	0·72	4·98	2·74	0·10	96·08
Volatile-free		77·71	11·94	0·22	1·13	0·12	0·75	5·18	2·85	0·10	100·00
602.80-E (E-type)	10	76·36	12·87	0·23	0·60	0·14	0·74	6·12	2·80	0·01	99·88
Volatile-free		76·45	12·89	0·23	0·60	0·14	0·74	6·13	2·80	0·01	100·00
UZN1663 (1663 lava)	20	71·67	12·48	0·96	2·81	0·18	0·77	3·79	5·30	0·07	97·73
Volatile-free		73·34	12·77	0·98	2·87	0·19	0·78	3·87	5·42	0·07	100·00

n, number of analyses averaged. Volatile-free indicates normalized to 100%.

may not be a true indicator of the temperature of the enclaves upon mixing with the host. Magnetite–ilmenite pairs analyzed in Equigranular enclaves are not zoned, and yield temperatures between 805° and 840°C, with an oxygen fugacity range of NNO + 0·25 to NNO + 1.

Quartz

Quartz typically accounts for 1–2 vol. % of dacite lavas, and always occurs as large, rounded and/or irregularly embayed phenocrysts with no reaction rim. Although rare, quartz occurs in Porphyritic enclaves and 1663 andesite, where a coarse-grained reaction rim of clinopyroxene, plagioclase, and glass invariably surrounds it.

Olivine

Olivine phenocrysts ($Fo_{65–75}$) range in size from 0·2 to 0·5 mm. Olivine may be found either as individual phenocrysts or glomeroporphyritic aggregates in Porphyritic enclaves (<1 vol. %). Olivine is not present in

Table 7: Representative electron microprobe (oxides in wt %) analyses of plagioclase along rim–core traverses

Sample	SiO_2	Al_2O_3	FeO	CaO	Na_2O	K_2O	Total	An
437.15-H (host lava), Plagioclase 1								
Rim	56·20	27·30	0·26	9·13	5·94	0·43	99·20	58·90
Middle	57·80	26·60	0·22	8·36	6·40	0·49	99·90	54·70
Core	57·70	26·40	0·22	8·25	6·42	0·51	99·60	54·30
602.80-H (host lava), Plagioclase 3								
Rim	58·90	25·20	0·88	7·74	5·28	0·48	98·50	56·90
Middle	55·10	28·20	0·48	10·13	4·72	0·26	98·90	66·10
Core	57·20	26·80	0·60	8·54	5·40	0·23	98·70	60·20
435.20-H (P-type), Plagioclase 5								
Rim	54·10	27·70	0·49	12·74	4·06	0·66	99·75	72·97
Middle	57·10	25·40	0·23	10·14	5·94	0·44	99·25	61·38
Core	56·90	27·10	0·21	8·85	6·18	0·42	99·66	57·28
62.50-E (P-type), Plagioclase 2								
Rim	52·90	29·00	0·41	11·54	4·55	0·27	98·70	70·10
Middle	55·40	26·70	0·28	9·10	5·85	0·38	97·70	59·30
Core	55·10	27·40	0·31	9·68	5·55	0·49	98·50	61·40
U2A-E (P-type), Plagioclase 1								
Rim	51·90	29·50	0·57	12·65	3·76	0·29	98·70	75·50
Middle	56·80	26·00	0·30	8·48	5·95	0·58	98·10	56·30
Core	54·80	27·60	0·22	9·91	5·65	0·31	98·50	62·40
262.50-E (P-type), Microphenocryst 1								
Rim	48·19	32·61	0·53	15·96	2·19	0·12	99·60	87·30
Middle	50·28	31·11	0·58	13·61	3·24	0·17	98·90	79·90
Core	56·80	26·90	0·28	9·09	5·89	0·33	99·30	59·40
435.20-E (P-type), Microphenocryst 1								
Rim	48·01	32·52	0·57	15·48	2·39	0·11	17·98	86·04
Middle	57·06	26·53	1·03	10·36	3·38	0·86	14·60	70·96
Core	62·44	22·89	0·97	7·87	3·54	1·54	12·95	60·07
390.00-E (E-type), Microphenocryst 3								
Rim	57·59	25·86	0·35	8·64	6·45	0·30	99·19	56·15
Middle	52·82	29·80	0·24	11·76	4·62	0·22	99·46	70·84
Core	49·60	31·63	0·15	14·52	3·32	0·14	99·37	80·76
390.00-E (E-type), Microphenocryst 2								
Rim	55·56	27·58	0·19	10·06	5·55	0·36	99·30	62·98
Middle	51·98	31·35	0·24	12·03	4·39	0·16	100·15	72·53
Core	48·64	31·37	0·37	15·15	3·03	0·14	98·71	82·69
UZN-1663 (1663 lava), Plagioclase B04a								
Rim	51·26	30·98	0·75	14·57	3·24	0·30	101·09	80·48
Middle	54·64	29·46	0·15	11·50	5·05	0·26	101·05	68·41
Core	51·61	31·43	0·37	14·09	3·75	0·19	101·43	78·16
UZN-1663 (1663 lava), Plagioclase A07								
Rim	48·30	33·58	0·48	16·82	2·19	0·07	101·44	88·17
Middle	57·16	27·63	0·22	9·46	6·01	0·36	100·85	59·74
Core	56·32	28·30	0·23	10·20	5·79	0·34	101·19	62·45

An, mol % anorthite.

Equigranular enclaves. Although olivine does occur as individual phenocrysts in the host lavas, it more commonly occurs in glomeroporphyritic aggregates with calcic plagioclase, clinopyroxene, and Fe–Ti oxides. Thin rims (<10 μm) of orthopyroxene typically surround olivine crystals in host lavas where in contact with surrounding matrix glass. Olivine crystals are usually unrimmed when observed in Porphyritic enclaves. Olivine is common in the 1663 lava, accounting for ~2 vol. % and ranging in composition from Fo_{60} to Fo_{75}. The 1663 lava olivine is slightly coarser-grained compared with that found in host lavas or Porphyritic enclaves, ranging in size from 0·2 to 1·2 mm. Olivine phenocrysts found in the 1663 lava are typically subhedral or anhedral and enclosed by a reaction rim of either hornblende or orthopyroxene where in contact with matrix glass.

Biotite

Biotite is sometimes found in the host lavas (<1 vol. %), and is invariably rimmed by pyroxene, plagioclase, and Fe–Ti oxides (± amphibole). Rarely, angular pieces of biotite grains that were probably fractured during ascent are found with reaction rims on only a few sides where in contact with groundmass. In Porphyritic enclaves, biotite is a rare mineral phase that is always surrounded by a fine-grained reaction rim of pyroxene, plagioclase, and Fe–Ti oxides. Biotite is not found in Equigranular enclaves or in the 1663 lava.

DISCUSSION

In this section, we first interpret the textural, petrological, and geochemical data presented above as strongly supporting a model for the origin of the Unzen magmas that involved mingling between basalt and dacite magma. Then, we propose a model to explain the formation of the texturally distinct enclaves in which Porphyritic enclaves are the product of rapid cooling at the boundary between mafic magma intrusions and host dacite magma, and Equigranular enclaves result from more prolonged development within the interior of the mafic magma intrusion. Finally, we argue that the mingling scenario presented here is widespread by briefly comparing examples from other volcanoes.

Mingling constraints from textural data

The textures of Porphyritic and Equigranular enclaves are distinct, suggesting that they experienced different cooling rates during formation. Porphyritic enclave texture indicates quenching of a largely liquid magma within a cooler silicic host as indicated by their acicular texture, chilled and cuspate margins, and an outward decrease in

Table 8: Representative electron microprobe analyses (oxides in wt %) of hornblende rims and cores

Sample:	103.80-H (host) HBL 2		103.80-E (E-type) Microphen. HBL 1		578.75-H (host) HBL 1		578.75-E (E-type) Microphen. HBL 3		262.80-H (host) HBL 2		262.80-E (P-type) Microphen. HBL 4	
	rim	core	rim	core	rim	core	rim	core	rim	core	rim	core
SiO_2	47·20	47·30	47·43	46·92	48·16	48·20	45·20	43·80	46·20	46·82	46·79	41·02
TiO_2	2·30	1·10	1·91	1·52	1·20	1·42	1·86	1·90	1·40	1·40	1·36	2·18
Al_2O_3	7·71	9·80	8·19	8·93	9·61	8·96	10·80	11·59	9·80	9·28	8·00	14·16
FeO*	13·15	10·89	11·14	11·01	10·44	11·11	10·85	10·20	11·82	11·20	11·68	10·73
Fe_2O_3*	1·81	4·25	3·49	3·13	3·95	2·53	3·81	3·98	3·08	3·51	2·85	3·97
MgO	13·97	14·72	14·65	14·71	14·91	14·83	14·51	15·39	14·18	14·92	14·33	14·20
CaO	11·40	9·48	9·88	10·52	9·16	9·97	9·46	9·97	10·26	10·28	10·17	10·48
Na_2O	1·28	1·21	1·19	1·34	1·38	2·19	1·80	2·08	1·48	1·38	1·32	2·20
K_2O	0·71	0·40	0·58	0·52	0·43	0·51	0·58	0·50	0·71	0·60	0·59	0·42
MnO	0·43	0·41	0·32	0·41	0·46	0·60	0·41	0·20	0·50	0·70	0·46	0·40
F	0·00	0·10	0·20	0·10	0·10	0·00	0·30	0·40	0·20	0·00	0·56	0·30
Cl	0·09	0·20	0·20	0·20	0·10	0·07	0·10	0·10	0·10	0·00	0·08	0·10
Total	100·05	99·86	99·18	99·31	99·90	100·39	99·68	100·11	99·73	100·09	98·19	100·16
Cations per 23 oxygens†												
Si	6·80	6·73	6·47	6·72	6·82	6·83	6·50	6·29	6·66	6·69	6·85	5·94
Al^{IV}	1·20	1·27	1·26	1·28	1·18	1·17	1·50	1·71	1·34	1·31	1·15	2·06
Ti	0·25	0·12	0·20	0·16	1·20	0·15	0·20	0·21	0·15	0·15	0·15	0·24
Al^{VI}	0·31	0·24	0·27	0·28	0·27	0·39	0·36	0·38	0·34	0·30	0·23	0·39
Fe^{2+}	1·58	1·30	1·32	1·44	1·24	1·32	1·30	1·22	1·42	1·34	1·43	1·30
Fe^{3+}	0·20	0·46	0·37	0·34	0·42	0·27	0·41	0·43	0·33	0·38	0·31	0·43
Mg	3·00	3·17	3·15	3·13	3·15	3·13	3·11	3·30	3·05	3·18	3·13	3·06
Mn	0·05	0·05	0·05	0·05	0·06	0·07	0·05	0·02	0·06	0·08	0·06	0·05
Ca	1·76	1·44	1·50	1·61	1·39	1·51	1·46	1·53	1·58	1·57	1·60	1·62
Na	0·18	0·17	0·16	0·19	0·19	0·30	0·25	0·29	0·21	0·19	0·19	0·31
K	0·13	0·07	0·11	0·10	0·08	0·09	0·11	0·09	0·13	0·11	0·11	0·08

*Ferrous and ferric iron calculated on the basis of 15 cations (after Robinson *et al.*, 1982).
†Structural formulae for all hornblendes calculated on the basis of 23 oxygens (after Helz, 1979).

grain size and increase in elongation of grains toward the enclave rim. This indicates an increase in crystal nucleation rate near the contact with the cooler host magma, and discredits the interpretation that they are the product of melting of a restite source or represent entrained cumulate material (Eichelberger, 1980). Basalt crystallization experiments have produced textures similar to those of Porphyritic enclaves, characterized by acicular and skeletal plagioclase, at undercooling conditions (ΔT) of between 140 and 185°C (Lofgren, 1980; Coombs *et al.*, 2002). This is consistent with an average difference in temperature between the Porphyritic enclaves and the host lava of 150°C, as determined in this study. The outward increase in glass content, strong normal zoning in microphenocrysts, and widespread occurrence of vesicles also implies rapid quenching.

Like Porphyritic enclaves, Equigranular enclaves contain a pervasive population of small single vesicles that exist in the irregular spaces between microphenocrysts, implying a vesiculation event induced by crystallization. Unlike Porphyritic enclaves, however, Equigranular enclave texture is consistent with a more gradual and prolonged crystallization history, as indicated by less steeply zoned and tabular to equant microphenocrysts that do not change in morphology with distance from the enclave rim. There is also the absence of chilled or crenulated margins, the enclave surface being characterized by protruding edges of microphenocrysts. Basalt crystallization experiments have produced similar textures with tabular crystal morphologies where undercooling was <40°C (Lofgren, 1980; Coombs *et al.*, 2002). This is consistent with an inferred temperature

Table 9: Representative electron microprobe analyses (oxides in wt %) of pyroxenes and olivines

Sample	SiO_2	TiO_2	Al_2O_3	Cr_2O_3	FeO	MnO	MgO	CaO	NiO	Total
153.85-H (host lava)										
OPX 2	52·19	0·21	1·40	0·02	21·20	0·11	23·86	1·01	0·00	100·00
OPX 3	51·70	0·09	1·21	0·02	21·68	0·32	23·02	1·03	0·03	99·10
OPX 6	51·67	0·19	1·49	0·02	19·62	0·86	25·26	1·43	0·03	100·57
199.90-H (host lava)										
OPX 1	52·40	0·11	0·80	0·03	21·26	1·40	23·85	0·53	0·01	100·39
OPX 2	52·70	0·08	0·80	0·02	20·81	1·30	24·19	0·59	0·40	100·89
U2A-E (P-type)										
OPX 1	53·83	0·14	1·56	0·17	14·24	0·40	28·97	1·41	0·01	100·73
OPX 2	54·06	0·11	0·73	0·19	13·84	0·61	29·22	1·32	0·05	100·13
CPX 1	49·85	0·75	3·63	0·23	7·68	0·24	15·77	20·40	0·00	98·55
CPX 2	50·98	0·55	3·22	0·37	5·93	0·21	17·64	20·77	0·06	99·73
Olivine 1	36·10	0·00	0·10	0·00	20·90	0·50	42·50	0·10	0·00	100·20
Olivine 2	37·70	0·06	0·00	0·10	20·10	0·18	41·90	0·00	0·00	100·04
153.85-E (E-type)										
OPX-1	51·56	0·15	1·66	0·08	21·50	1·08	23·43	0·88	0·11	100·45
OPX-2	51·44	0·29	0·84	0·04	21·39	1·49	24·06	0·73	0·02	100·30
262.80-E (E-type)										
OPX 1	50·30	0·20	1·50	0·00	21·30	1·00	21·20	1·30	0·00	96·80
OPX 3	52·50	0·10	0·40	0·00	22·90	1·50	22·50	0·70	0·00	100·60
CPX 1	51·60	0·40	2·70	0·30	5·70	0·10	18·20	20·60	0·00	99·60
CPX 2	51·20	0·70	3·10	0·00	8·50	0·40	18·10	17·70	0·00	99·70
CPX 4	51·20	0·80	5·20	0·10	8·10	0·30	14·50	17·30	0·10	97·60
Olivine 1	38·48	0·04	0·08	0·01	17·25	0·24	43·62	0·10	0·11	99·93
Olivine 2	39·21	0·07	0·42	0·04	18·28	0·36	42·02	0·18	0·14	100·72
Olivine 4	38·16	0·03	0·10	0·02	17·18	0·28	44·71	0·08	0·11	100·67
199.90-E (E-type)										
OPX 3	52·60	0·10	0·70	0·00	21·10	1·40	23·80	0·60	0·00	100·30
OPX 4	52·40	0·10	0·90	0·00	21·40	1·40	23·90	0·50	0·00	100·60
602.80-E (E-type)										
OPX 1	51·85	0·14	0·83	0·05	21·67	1·37	23·58	0·69	0·02	100·20
OPX 2	52·13	0·20	1·05	0·00	19·81	0·72	24·72	0·91	0·04	99·58
OPX 5	52·01	0·15	0·85	0·04	20·75	1·14	23·70	0·73	0·04	99·41
UZN1663 (1663 Lava)										
OPX 1	53·40	0·45	1·72	0·00	17·33	0·48	23·74	2·36	0·01	99·48
OPX 2	53·90	0·35	2·42	0·00	14·37	0·42	25·61	2·26	0·04	99·37
CPX 1	51·73	0·38	1·94	0·00	5·93	0·23	17·59	19·28	0·00	97·08
CPX 2	52·25	0·55	3·05	0·10	7·50	0·22	18·29	17·57	0·00	99·54
CPX 3	53·24	0·46	1·45	0·00	9·51	0·43	17·40	17·35	0·04	99·87
CPX 4	51·10	0·70	3·38	0·00	8·74	0·37	16·62	17·89	0·00	98·80
CPX 5	50·30	1·29	5·26	0·00	7·88	0·28	16·96	17·39	0·00	99·35
Olivine 1	38·18	0·02	0·00	0·20	23·46	0·44	37·59	0·09	0·16	100·15
Olivine 2	38·18	0·01	0·03	0·10	24·05	0·30	36·81	0·12	0·15	99·75
Olivine 3	39·20	0·01	0·02	0·10	19·74	0·34	40·94	0·11	0·15	100·61
Olivine 4	39·31	0·03	0·03	0·00	18·79	0·36	41·96	0·06	0·14	100·67
Olivine 5	38·74	0·02	0·03	0·30	21·69	0·37	38·94	0·06	0·14	100·28

Table 10: Representative electron microprobe analyses (oxides in wt %) of magnetite and ilmenite pairs

Sample		TiO_2	Al_2O_3	Cr_2O_3	FeO	MnO	MgO	NiO	V_2O_3	CaO	Total	Usp	Ilm	T (°C)	log fO_2
199.10-H (host lava)															
Magnetite	core	5·90	0·80	0·10	89·40	0·50	1·80	0·08	0·64	0·06	99·28	0·16			
Ilmenite	core	39·30	0·10	0·00	54·20	0·70	1·80	0·02	0·24	0·05	96·41		0·87	806°C ± 20	−11·76
Magnetite	rim	9·50	1·15	0·00	86·49	0·58	1·15	0·04	0·38	0·04	99·34	0·26			
Ilmenite	rim	43·20	0·10	0·00	51·85	0·76	2·18	0·04	0·45	0·03	98·61		0·81	850°C ± 20	−11·79
390.00-H (host lava)															
Magnetite	core	5·90	1·60	0·10	89·08	0·60	1·79	0·10	0·59	0·04	99·80	0·17			
Ilmenite	core	42·20	0·10	0·00	55·50	0·60	1·80	0·04	0·28	0·04	100·56		0·90	810°C ± 15	−11·71
Magnetite	rim	9·30	0·80	0·00	86·70	0·60	1·78	0·04	0·44	0·04	99·70	0·26			
Ilmenite	rim	44·50	0·10	0·00	51·20	0·60	2·10	0·04	0·39	0·04	98·97		0·79	839°C ± 20	−11·93
602.80-H (host lava)															
Magnetite	core	6·70	0·66	0·11	89·40	0·44	1·21	0·09	0·39	0·09	99·09	0·18			
Ilmenite	core	41·00	0·00	0·00	55·80	0·50	2·20	0·04	0·29	0·04	99·87		0·83	803°C ± 25	−12·17
Magnetite	rim	7·60	0·78	0·00	88·70	0·44	1·22	0·04	0·29	0·09	99·16	0·21			
Ilmenite	rim	41·20	0·10	0·00	55·10	0·70	2·10	0·04	0·34	0·04	99·62		0·83	826°C ± 15	−11·87
262.50-E (P-type)															
Magnetite	core	10·90	1·70	0·00	84·40	0·60	2·14	0·09	0·68	0·05	100·56	0·33			
Ilmenite	core	41·20	0·20	0·10	55·90	0·50	0·10	0·04	0·24	0·04	98·32		0·83	925°C ± 20	−10·43
Magnetite	rim	9·40	0·80	0·20	86·40	0·40	1·90	0·04	0·59	0·04	99·77	0·21			
Ilmenite	rim	41·20	0·11	0·00	54·60	0·54	1·92	0·04	0·24	0·04	98·69		0·86	831°C ± 20	−11·68
U2A-E (P-type)															
Magnetite	core	9·70	2·40	0·30	84·40	0·60	1·90	0·09	0·48	0·09	99·96	0·56			
Ilmenite	core	44·30	0·10	0·10	53·60	0·60	1·20	0·04	0·04	0·04	100·02		0·77	1040°C ± 25	−9·84
Magnetite	rim	9·20	1·90	0·00	85·60	0·50	1·40	0·04	0·54	0·04	99·22	0·26			
Ilmenite	rim	42·10	0·10	0·00	55·60	0·70	1·80	0·04	0·04	0·04	100·42		0·89	895°C ± 25	−10·90
199.10-E (E-type)															
Magnetite	core	7·70	1·74	0·10	88·50	0·40	1·20	0·08	0·38	0·04	100·14	0·21			
Ilmenite	core	40·20	0·20	0·00	57·40	0·60	2·20	0·04	0·21	0·04	100·89		0·96	840°C ± 15	−11·13
Magnetite	rim	7·60	1·41	0·10	88·60	0·50	1·30	0·04	0·31	0·04	99·90	0·21			
Ilmenite	rim	43·20	0·10	0·00	52·85	0·76	2·18	0·04	0·14	0·04	99·31		0·82	837°C ± 20	−11·96
390.00-E (E-type)															
Magnetite	core	6·30	1·84	0·10	89·80	0·50	1·20	0·04	0·46	0·04	100·28	0·17			
Ilmenite	core	41·60	0·10	0·10	55·60	0·60	1·50	0·04	0·28	0·04	99·86		0·89	815°C ± 20	−11·65
Magnetite	rim	6·10	1·40	0·00	88·90	0·50	1·20	0·04	0·39	0·04	98·57	0·17			
Ilmenite	rim	41·20	0·10	0·00	55·50	0·60	1·80	0·04	0·18	0·04	99·46		0·90	810°C ± 25	−11·73

Temperatures and oxygen fugacities calculated using the Anderson & Lindsley (1988) algorithm. All oxides reported in wt %; Usp, mol % ulvöspinel; Ilm, mol % ilmenite.

difference between the Equigranular enclaves and host lavas of 10–45°C. Finally, it is important to note that the characteristic Porphyritic enclave texture does not occur as a rind on Equigranular enclaves. This indicates that the differences between the two texturally distinct enclaves cannot be due merely to size (diffusion path-length) dependence, resulting from direct contact with the host lava on the exterior of enclaves producing a Porphyritic texture with the Equigranular enclave texture developing in their interiors.

Mingling constraints from petrological data

Plagioclase microphenocrysts, with calcic core compositions ranging from An_{75} to An_{90}, are the dominant phase in both types of Unzen enclave. This suggests that

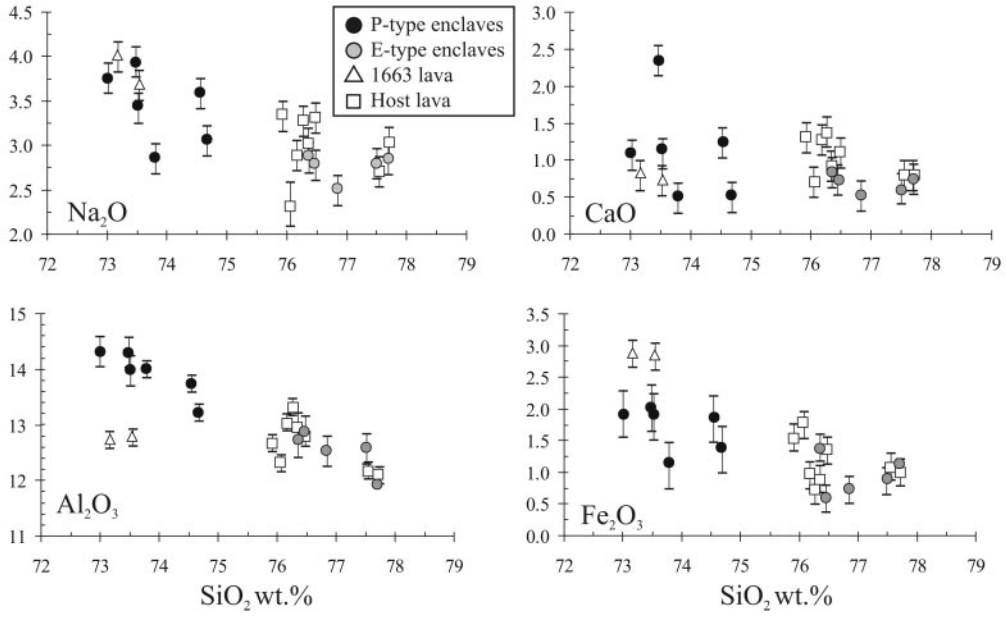

Fig. 11. Major oxide–SiO_2 variation in matrix glass (with 2σ error bars) for host lava (□), Porphyritic enclaves (●), Equigranular enclaves (◉) and 1663 lava (△).

microphenocryst plagioclase crystallized from the enclave-forming magma. The interiors of plagioclase phenocrysts from Porphyritic enclaves, however, are typically oscillatory zoned and have An compositions identical to interiors of plagioclase grains in the host lavas, which are too sodic have been precipitated from the enclave-forming magma. Furthermore, sodic plagioclase phenocryst cores in Porphyritic enclaves are invariably surrounded by resorption zones that cut across oscillatory zoning profiles. These zones strongly resemble experimentally developed resorption zones on plagioclase grains that formed in response to sudden heating events (Tsuchiyama & Takahashi, 1983; Tsuchiyama, 1985; Nakamura & Shimakita, 1998). We interpret the Porphyritic enclave plagioclase phenocrysts to have originated from the host magma and that the resorption zones record the mineralogical response to the abrupt change in surrounding melt composition and temperature from which the sodic oscillatory-zoned interior precipitated.

The presence of host-derived phenocrysts in Porphyritic enclaves requires that intruding mafic magma engulfed plagioclase phenocrysts from the host dacite magma during replenishment events. The thickness of resorption zones can be used to constrain the amount of time required for engulfment of host magma by intruding basaltic magma to occur. Resorption zones on sodic Porphyritic enclave plagioclase phenocrysts range in thickness from 30 to 500 μm. Development of zones with this range in thickness requires 0·3–8 days given a surrounding temperature range of between 950 and 1050°C according to experiments (Tsuchiyama & Takahashi, 1983; Tsuchiyama, 1985; Nakamura & Shimakita, 1998). But does intruding basalt engulf host magma while in the form of enclaves? A simple conduction model predicts that a 30 cm diameter enclave at 1000°C would approach thermal equilibration with the surrounding host magma (800°C) in an hour (e.g. Jaeger, 1968). This suggests that the host magma probably does not mix with the intruding basalt while in the form of blobs or enclaves because rapid cooling leaves insufficient time for the resorption zones to form. Thus much of the development of the resorption zones on host-derived plagioclase probably occurred when they were incorporated into the mafic intrusion, and completed formation as the mixed magma was dispersed.

Equigranular enclaves do not contain vestiges of incorporated crystalline phases from the host like the Porphyritic enclaves, nor do they contain olivine. In addition, Equigranular enclaves interstitial melt was in chemical equilibrium with (i.e. identical in composition to) the melt of the host. Why then, are they more equilibrated than the Porphyritic enclaves? One possibility is that the Equigranular enclaves are derived from a third andesitic magma, different from the magma that formed the Porphyritic enclaves. We reject this hypothesis because of the strong chemical resemblance between the Equigranular enclaves and the obviously hybrid Porphyritic enclaves. In addition, eruptions at Unzen appear to be generated by mafic inputs to the system. For three magma batches to repeatedly participate in generating eruption products seems like a colossal coincidence. We also reject

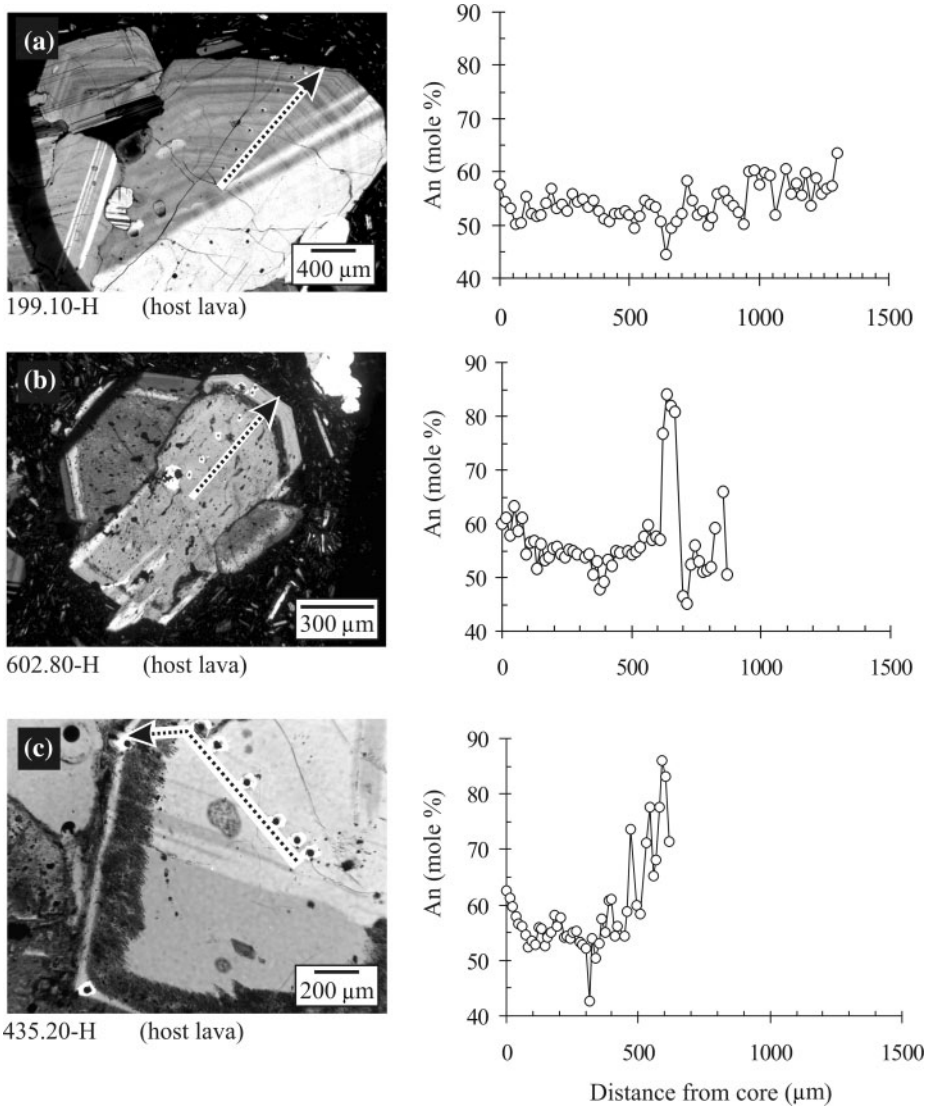

Fig. 12. Photomicrographs of the three populations (see text) of plagioclase phenocrysts from the host lavas (a, 199.10-H; b, 602.80-H; c, 435.20-H) and mol % An (open symbols) along core to rim sampling transects. Arrows indicate path of sampling transects for electron microprobe analyses.

the hypothesis that Equigranular enclaves are cumulates, because cumulate products of magma would contain the same phases that the magma is precipitating. However, the crystal phases in the Equigranular enclaves differ in their composition and morphology from crystal phases in the dacite magma.

We, therefore, argue that Equigranular enclaves are basalt + dacite hybrids, as indicated by calcic plagioclase microphenocrysts ($An_{75–85}$), elevated crystallization temperatures compared with the host, abundant vesicles, and strong bulk chemical resemblance to the Porphyritic enclaves. Accepting this inference that enclaves are hybrids nonetheless requires an explanation for why they are more equilibrated than the Porphyritic enclaves. One possibility is that they are simply Porphyritic enclaves from previous replenishment events that have ripened with time. This argument appears to explain the presence of the enclaves with textures intermediate to Porphyritic and Equigranular types, but can be rejected as the general mode of formation for Equigranular enclaves for several reasons. First, if Equigranular enclaves were the disaggregated remnants of Porphyritic enclaves, one would expect to find cores of engulfed host phenocrysts within Equigranular enclaves. Longer residence times within the cool dacitic magma would not result in the destruction of engulfed phenocrysts in aged Porphyritic enclaves, for the cores of those phenocrysts are already in equilibrium with the host. Second, the majority of Unzen enclaves can be easily distinguished as either Porphyritic or Equigranular based on texture. If Equigranular enclaves were the

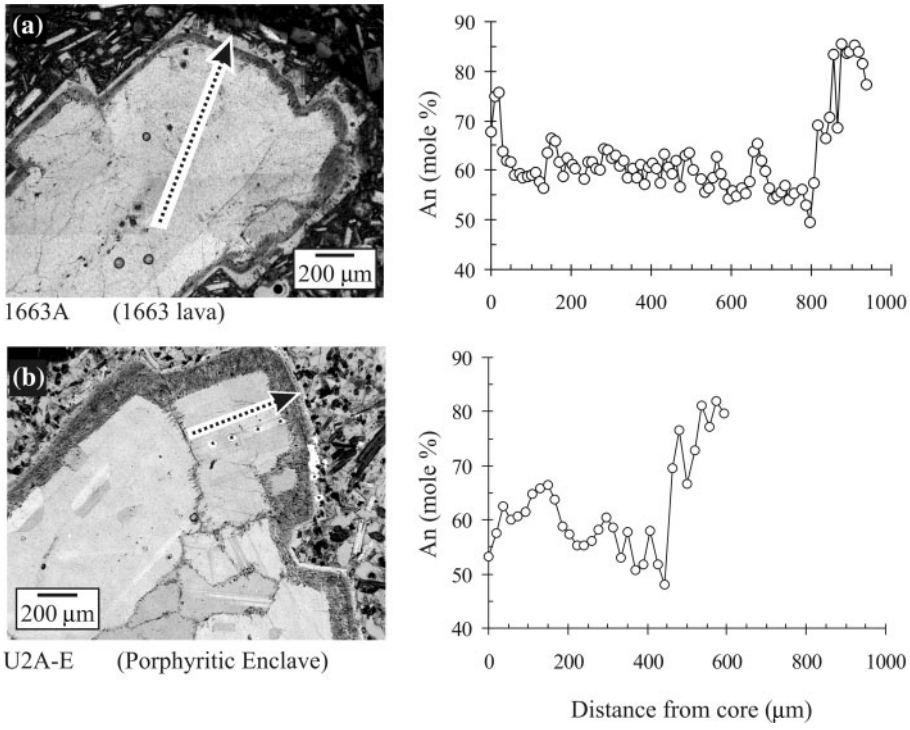

Fig. 13. Photomicrographs of plagioclase phenocrysts from (a) the 1663 lava and (b) Porphyritic enclaves (U2A-E) and mol % An (open symbols) along core to rim sampling transects. Arrows indicate path of sampling transects for electron microprobe analyses.

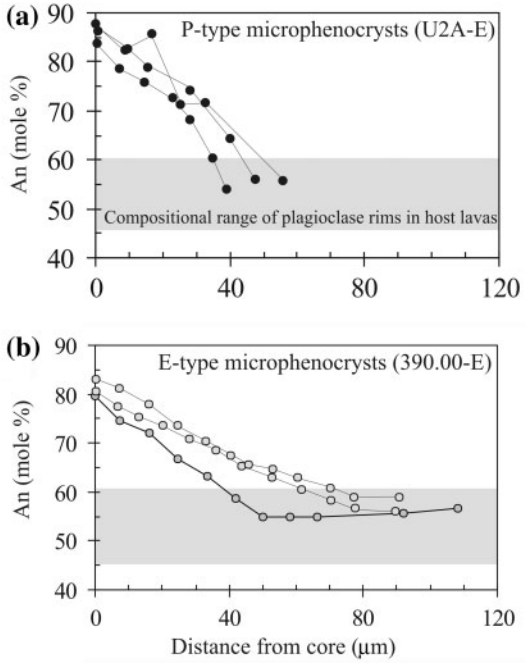

Fig. 14. Compositional zoning (mol % An) in selected samples of microphenocryst plagioclase from Porphyritic (a, U2A-E, closed symbols) and Equigranular enclaves (b, 390.00-E, open symbols) along core to rim transects. Shaded region on graphs represents the range of composition for the rims of coexisting plagioclase phenocrysts in the host lava.

disaggregated remnants of Porphyritic enclaves one would expect to find a wide range of textures between them, but intermediary enclaves occur only in trace amounts in the host lavas. Third, it is unlikely that the acicular and steeply normally zoned microphenocrystic plagioclase in Porphyritic enclaves would evolve into tabular microphenocrysts with more gradual zoning over time.

Mingling constraints from geochemical data

Many of the compositional arrays of Unzen lavas and Porphyritic enclaves are broadly linear (e.g. Fe, Ca, Y) over nearly 15 wt % range in SiO_2, which supports a mixing relationship between basalt and dacite end-members. Some elemental arrays, however, are scattered (e.g. Ba, Sr, P) or curvilinear (e.g. Al, Na). This suggests that processes such as crystallization, fractionation, and assimilation probably operate in the Unzen magma reservoir between mafic intrusions over time. Compositional scatter is also apparent among the Equigranular enclaves, which probably resulted from their small size (averaging ~2 cm in diameter) relative to grain size. In addition, some Porphyritic enclave elemental trends project to compositions that are depleted beyond host lava compositions (e.g. Sr, Ba, Rb), suggesting that enclaves may have experienced some separate form of crystal–liquid

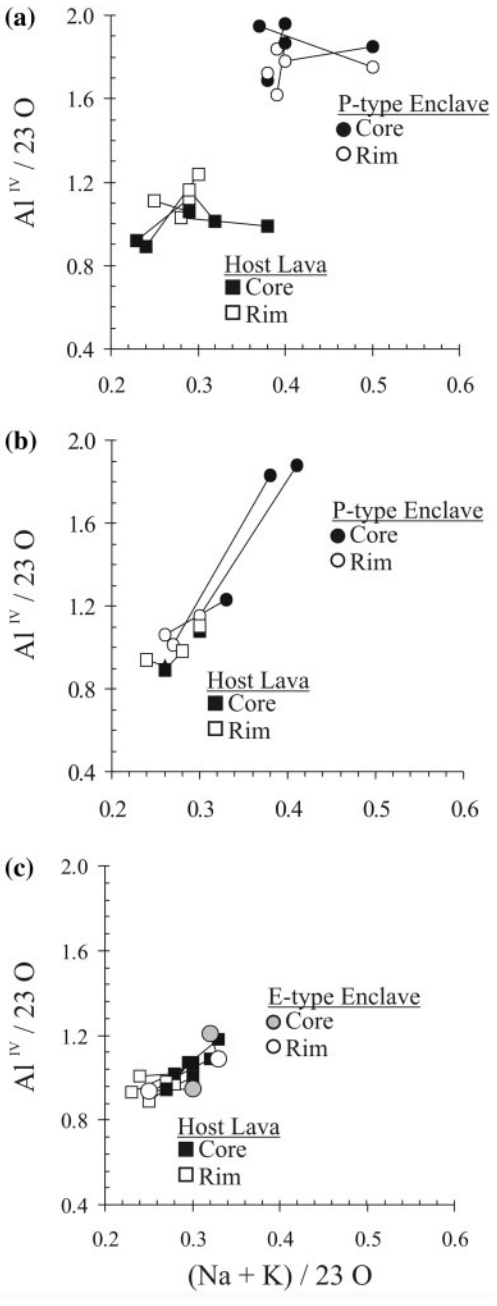

Fig. 15. Al^{IV} vs Na + K in coexisting hornblende crystals in enclaves and their host lavas. (a) Porphyritic enclave and host (U3A-H, U3A-E); (b) Porphyritic enclave and host (578.75-H, 578.80-E); (c) Equigranular enclave and host (103.80-H, 103.80-E). Lines connect intra-grain analyses. All structural formulae calculated on the basis of 23 oxygens (after Helz, 1979) and 15 cations (after Robinson *et al.*, 1982).

differentiation, such as gas-driven filter pressing (Anderson *et al.*, 1984; Sisson & Bacon, 1999). Porphyritic enclaves do not contain segregation pipes of rhyolitic melt, however, which might be expected if filter pressing had occurred (e.g. Bacon, 1986).

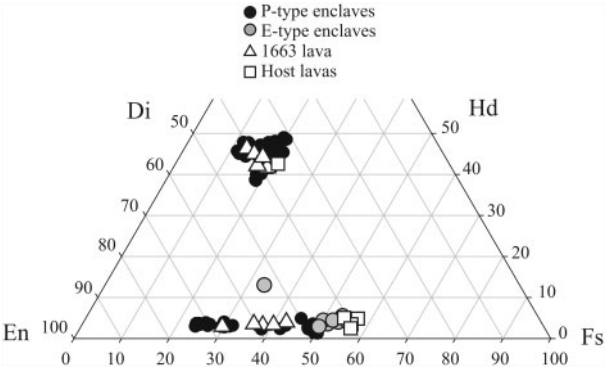

Fig. 16. Pyroxene compositions in host lavas (□), Porphyritic enclaves (●), Equigranular enclaves (◉), and 1663 lava (△).

Projection of the mixing lines yields information on the compositions of possible end-members, though subject to the above uncertainties. The most silicic host dacite lava samples have a composition between 64 and 65 wt % SiO_2, although even these samples contain abundant evidence of mixing such as the presence of enclaves, recycled phenocrysts, and coexistence of quartz and olivine. Holtz *et al.* (2005) postulated a silicic end-member composition of ~70 wt % SiO_2 (with 8 ± 1 wt % H_2O), based on melt inclusion compositions from phenocrysts in host lavas. Findings from this study, however, show that the host lavas are widely populated with crystal phases of diverse and complex crystallization and melting histories, making the interpretation of phenocryst melt inclusion data difficult. Therefore, we prefer to estimate a silicic end-member component with a SiO_2 content of ~66 wt % for the purposes of mixing calculations.

With regard to the mafic component, previous studies have used the 1663 lava in mixing models (e.g. Chen *et al.*, 1999; Nakada & Motomura, 1999); this contains ~57 wt % SiO_2. Another candidate for the mafic end-member is the most mafic Porphyritic enclave, which contains ~51 wt % SiO_2. Most recently, Holtz *et al.* (2005) suggested an aphyric mafic end-member with ~60 wt % SiO_2 (with 4 ± 1 wt % H_2O) based on graphical extrapolations between a hypothetical silicic end-member (see above) and the groundmass compositions of enclaves. However, neither of these candidates can accurately represent a mafic mingling end-member for several reasons: (1) both the 1663 lava and the most mafic Porphyritic enclave contain abundant host-derived phenocrysts, which require some degree of mixing prior to quenching; (2) a larger proportion of the incorporated host-derived rhyolite liquid component undoubtedly accompanies the engulfment of host phenocrysts into the enclave-forming magma into the groundmass, which also requires mixing prior to quenching; (3) all Porphyritic and Equigranular enclaves analyzed in this study,

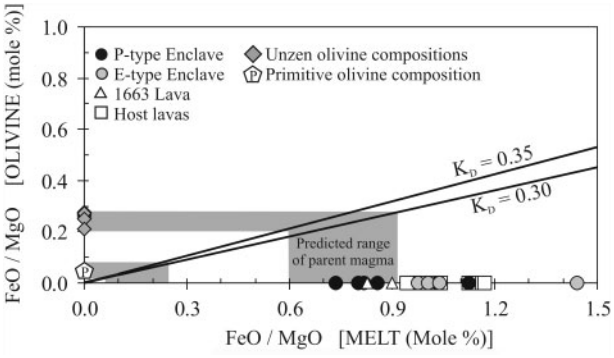

Fig. 17. The measured FeO/MgO ratio (mol %) in olivine crystals (shaded diamonds) found in Porphyritic enclaves, host lavas, and the 1663 lava plotted against the measured FeO/MgO ratio (mol %) for whole-rock compositions of the Porphyritic enclave (●), Equigranular enclaves (◉), host lavas (□), and 1663 lava (△). It should be noted that Unzen olivine compositions are consistent only with the calculated FeO/MgO ratios (mol %) for Porphyritic enclave and the 1663 andesite melts, given a range of distribution coefficients (K_D) for the exchange of Fe and Mg between olivine and coexisting melt of 0·30 and 0·35 (Roeder & Emslie, 1970; Ulmer, 1989). The difference between Unzen olivine compositions and olivines found in primitive magmas should also be noted (data from Clynne & Borg, 1997).

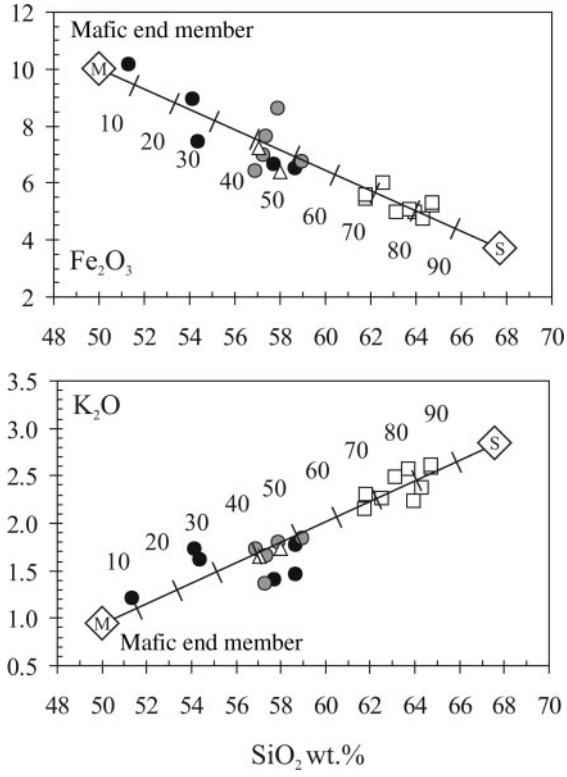

Fig. 18. Mixing line showing proportions of a mafic (M) and silicic (S) end-member in Unzen host lavas, P-type and E-type enclaves, and the 1663 lava flow plotted on Fe_2O_3 and K_2O vs SiO_2 variation diagrams. Tick marks on mixing lines indicate weight percent of the silicic end-member. (See text for discussion of mixing end-member compositions.) Symbols as in Fig. 17.

which contain abundant evidence for mixing with the host magma, are more mafic than the end-member proposed by Holtz *et al.* (2005).

One proxy for the mafic end-member is to analyze olivine crystals present in Porphyritic enclaves and Unzen lavas. Although olivines are usually unrimmed in Porphyritic enclaves, they are clearly unstable in the Unzen host lavas and the 1663 lava, as evidenced by reaction rims of orthopyroxene or hornblende where crystal faces are in contact with the matrix glass. Olivine compositions from enclaves and lavas range from Fo_{65} to Fo_{75}, which is common for olivine in high-aluminum basaltic magmas from andesitic arcs.

After accounting for oxygen fugacity, based on touching magnetite–ilmenite pairs, to calculate the correct proportions of Fe^{2+} and Fe^{3+} in olivine and glasses (e.g. Sack *et al.*, 1980), the exchange equilibria of Mg and Fe^{2+} between olivine and melt (Roeder & Emslie, 1970) indicate that the Unzen residual olivines crystallized from a basaltic melt with a range of FeO/MgO (mol %) ratios between 0·6 and 0·9. The calculated FeO/MgO (mol %) ratios for melts equivalent to the bulk composition of the Porphyritic enclaves and the 1663 andesite range from 0·75 to 1·1, which is consistent only with the most evolved Unzen olivine compositions (Fig. 17). The most primitive olivines could not be precipitated from the most primitive enclave, which has 51 wt % SiO_2 and itself shows evidence of hybridization. Therefore, we estimate the mafic end-member to have a SiO_2 content of ~50 wt % for the purposes of mixing calculations based on the correlation of the most primitive predicted FeO/MgO (mol %) melt ratio (0·6) and mixing trend from the silicic end-member. This is clearly not a 'primitive' basaltic composition indicative of direct mantle derivation (Luhr & Carmichael, 1985; Bacon *et al.*, 1997; Clynne & Borg, 1997), implying that the intruding basalt end-member evolved substantially since extraction from the mantle and prior to intrusion into the Unzen magma reservoir—perhaps in a region at the crust–mantle boundary beneath Tachibana Bay, where the pre-eruption seismicity began (Nakada *et al.*, 1999).

Estimates of the proportion of end-member magmas in Unzen lavas and enclave types suggest that both products of mingling are significantly hybridized (Fig. 18). Porphyritic enclaves contain a wide range of proportions of the silicic end-member from 5 to 55 wt %. In contrast, the Equigranular enclaves and 1663 andesite are made from nearly equal proportions of each end-member, ranging from 45 to 55 wt % silicic end-member component. Finally, the host lavas contain between 10 and 25 wt % of the mafic end-member. These high mixing proportions are consistent with the disequilibrium mineral assemblage of Unzen lavas and enclaves in which reaction rims and embayed and/or partially dissolved crystal

faces on quartz and albitic-cored plagioclase exist in the Porphyritic enclaves, and olivine and clinopyroxene exist in the Unzen lavas.

Mingling model

The occurrence of the two textural enclave types together in all enclave-bearing lavas erupted from Unzen suggests that we might look for conditions that could give rise to both during a single intrusive event. The textural, petrologic, and geochemical differences between Equigranular and Porphyritic enclaves are interpreted to be the result of different, but not necessarily exclusive, modes of formation (Fig. 19). We propose that replenishment events at Unzen are characterized by the intrusion of high-alumina olivine-bearing basaltic magma into the base of a silicic magma chamber (e.g. Wiebe, 1994; Snyder & Tait, 1995; Fig. 19a). Upon and during intrusion, the replenishing basalt engulfs, assimilates, and mixes with portions of the resident silicic magma. The intruded magma, now an andesite hybrid, experiences rapid crystallization and subsequent second boiling in response to heat loss into the overlying silicic host magma (Huppert *et al.*, 1982*b*; Jaupart & Vergniolle, 1989). As a result, blobs of andesitic hybrid rise buoyantly into the overlying host magma—accelerating the cooling and crystallization process (Eichelberger, 1980; Huppert *et al.*, 1982*a*) (Fig. 19b). These become Porphyritic enclaves. Second boiling also results in degassing of the intruded mafic magma, which is consistent with the recent findings of Sato *et al.* (2005).

Meanwhile, the temperature contrast between the hybridizing intrusion and resident silicic host magma decreases. The intrusion cools through mixing with, and conduction to, the overlying cool silicic magma. The silicic magma above the interface is warmed through conduction and by incorporation of disrupted mafic material (Fig. 19c). While the degree of undercooling and second boiling that drives the underlying hybrid to buoyantly rise as vesicular enclaves into the host magma diminishes, the interior of the mafic intrusion slowly crystallizes as a framework of equigranular crystals in a vesicular matrix (Fig. 19c). This slower cooling permits thorough homogenization and hence the more limited range in composition. It also allows time for thorough digestion, rather than merely resorption, of engulfed phenocrysts from the silicic magma and dissolution of olivine inherited from the basalt.

Equigranular enclave clots are stripped off the cooling intrusion by convective stirring, or perhaps disrupted during subsequent replenishment events (Fig. 19d). Equigranular enclaves are subsequently dispersed throughout the host magma. Some may be engulfed by subsequent intrusion events as indicated by their occasional presence in Porphyritic enclaves. In examples of mafic intrusions in silicic plutons, the volume of the mafic

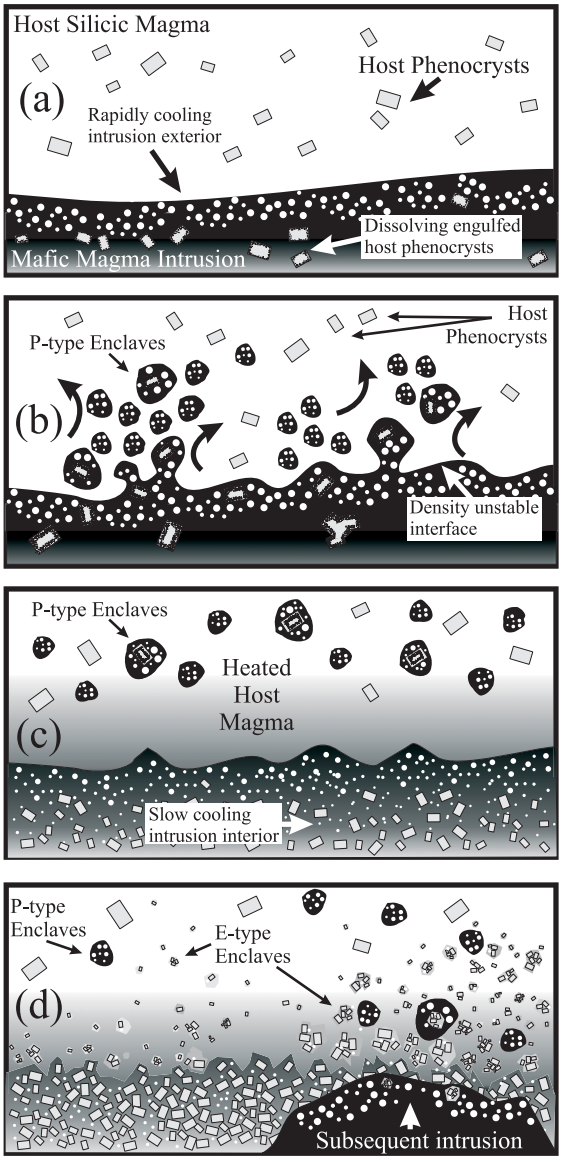

Fig. 19. Schematic model for the formation of Porphyritic and Equigranular enclaves in the Unzen magma chamber. Upon and during intrusion of high-alumina olivine-bearing basaltic magma into the base of the Unzen silicic magma chamber, the replenishing basalt engulfs and assimilates host magma (melt + phenocrysts) (a). The intruded magma experiences rapid crystallization and subsequent second boiling in response to heat loss into overlying silicic host magma (b), which generates Porphyritic enclaves through the buoyant rise of hybrid blobs into the overlying host magma. The overlying host magma is warmed through conduction and by incorporation of P-type enclaves as the interior of the mafic intrusion slowly crystallizes as a framework of equigranular crystals in a vesicular matrix. This facilitates more thorough digestion, rather than merely resorption, of engulfed phenocrysts from the silicic magma and dissolution of olivine inherited from the basalt. (c). Equigranular enclave clots are stripped off the cooling intrusion by convective stirring, or perhaps disrupted during subsequent replenishment events and are subsequently dispersed throughout the host magma (d). Some E-type enclaves are also engulfed by subsequent intrusion events as indicated by their occasional presence in Porphyritic enclaves. (See text for further discussion.)

intrusion interior typically exceeds the quenched exterior (e.g. Wiebe *et al.*, 2002). This is consistent with Equigranular enclaves being 2–5 times more abundant than Porphyritic ones.

The 1663 lava is anomalous because it contains no enclaves of either textural type. It is also chemically unique for lavas in that its composition plots at the silicic end of the enclave field, where mixing calculations indicate that it results from a nearly 1:1 mixture of mafic and silicic end-members. Given the similarity of 1663 lava to the Porphyritic enclaves, in terms of both bulk composition and disequilibrium phenocryst assemblage, we argue that the two differ only in post-mixing thermal history. Whereas the Porphyritic enclaves represent the hybrid magma from the mafic–silicic interface that was dispersed and quenched in the host dacite, the 1663 lava represents an eruption of hybrid magma directly from the mafic–silicic interface without the typical steps of dispersal and quenching in the silicic resident magma.

Variation of the mingling model

We have emphasized the intrusion of mafic magma in lava flow-like form (Wiebe, 1994; Snyder & Tait, 1995); however, mafic magma may also replenish silicic reservoirs vigorously as a low-viscosity, bubble-rich fluid, as a result of CO_2-rich vapor exsolution prior to injection (e.g. Phillips & Woods, 2001). Instead of ponding at the base of the chamber, such a model predicts that a turbulent plume will be generated upon initial injection, subsequently subsiding to produce a flow that cools relatively slowly on the floor of the chamber. In such a case, Porphyritic enclaves might represent quenched blobs in the turbulent 'spray' from the basalt plume, and Equigranular enclaves might be produced by slow cooling of the flow on the magma chamber floor. This model is consistent with observations from Unzen, such as: (1) widespread distribution of mafic phenocrysts and enclaves in the host lavas; (2) the lack of intermediary enclave textures, for two distinct mingling mechanisms would probably produce two unique textures; (3) the large range in size for Porphyritic enclaves (5–30 cm), which might be expected from a chaotic and turbulent plume; (4), the large coalesced vesicles in Porphyritic enclaves, suggestive of two episodes of vesiculation, one prior to intrusion as a result of the exsolution of CO_2-rich vapor.

The crystallization of the intruded mafic magma is not an instantaneous response to cooling, however. If it were, little or no mingling would occur. For example, experimental results cited previously indicate that 0·3–8 days are required for the growth of resorption zones, of equivalent thickness, on incorporated sodic plagioclase, to those observed in Unzen Porphyritic enclaves. This implies that a 'spray model' origin for Unzen enclaves is unlikely because of the required time for resorption zone formation and microphenocryst growth. We concede, however, that if resorption and crystallization actually occur faster than experimentally observed thus far, for example because the resorption occurs at higher temperature, the spray model could be viable.

Mingling implications

Enclave-bearing lavas from some volcanoes preferentially contain enclaves of one texture. For example, lavas erupted from Augustine volcano, Alaska, almost exclusively contain enclaves with porphyritic texture (Swanson, 1993). Conversely, lavas erupted from Pinatubo volcano, Philippines, preferentially contain enclaves that are equigranular (Pallister *et al.*, 1996). Nonetheless, both textural types are ubiquitous in the enclave-bearing lavas of Unzen, and are commonly found in enclave-bearing lavas elsewhere, such as Mount Lassen, California (Heiken & Eichelberger, 1980), Mount Dutton, Alaska (Miller *et al.*, 1999), and Kizimen Volcano, Kamchatka (Melekestsev *et al.*, 1995). Wiebe (1994) and Wiebe *et al.* (2002) also observed texturally similar types of enclaves in plutonic rocks. This strongly suggests that both textural enclave types are probably products of interaction of the same magma, resulting from different styles of magma mingling during the same or successive mafic replenishment events. We have suggested one way in which this could occur during a single replenishment event.

CONCLUSIONS

(1) All erupted products from Mount Unzen record replenishment events of high-aluminum olivine basalt magma into the silicic magma reservoir, as indicated by abundant and evenly distributed magmatic enclaves, disequilibrium phenocryst assemblages, and textures of both host and enclave-free lavas.

(2) Magmatic enclaves are divided into two texturally distinct groups, Porphyritic and Equigranular. The texture, petrology, and geochemistry of Porphyritic enclaves indicate that they experienced rapid cooling at the interface between intruded basalt and silicic magma, whereas Equigranular enclaves crystallized more slowly in the interior of the mafic intrusion.

(3) Even the most silicic host dacite lavas (~65 wt % SiO_2) and mafic Porphyritic enclaves (~51 wt % SiO_2) contain evidence of contamination, therefore silicic (~66 wt % SiO_2) and mafic (~50 wt % SiO_2) end-members are assumed for mixing calculations. Significant incorporation of both end-member magmas is necessary to explain the observed compositions; Porphyritic enclaves contain 5–55 wt % silicic component, Equigranular enclaves and the 1663 andesite contain

nearly equal proportions of each end-member, and the host lavas contain between 10 and 25 wt % mafic end-member.

(4) Replenishment events at Unzen are characterized by the intrusion of high-alumina olivine-bearing basaltic magma into the base of a silicic host magma chamber, engulfing and mixing with portions of the surrounding host melt and phenocrysts. The intruded magma, now an andesitic hybrid, experiences rapid crystallization and subsequent second boiling in response to heat loss into the overlying silicic host magma. As a result, the hybrid rises buoyantly into the host magma, quenching in the cooler silicic host. The interior of the hybrid intrusion, however, cools more slowly, resulting in a crystallized framework of equigranular, tabular crystals in a poorly vesicular matrix. Equigranular enclaves and crystal clots are disrupted, stripped off, and subsequently dispersed in the host magma as a result of convective stirring or simply detaching along the preferentially weak zones of the microphenocryst framework. Equigranular enclaves may also be disrupted and subsequently engulfed by successive intrusion events.

(5) Both textural types of enclaves observed at Unzen are common in enclave-bearing lavas erupted from other volcanoes including Mount Lassen, Mount Dutton, and Kizimen volcano. Wiebe (1994) and Wiebe *et al.* (2002) also observed both types of enclaves in plutonic rocks, suggesting that both textural enclave types are products of the same magma, resulting from different styles of magma mingling during the same or successive mafic replenishment events.

(6) Our above observations are important in highlighting the open-system nature of many arc volcanic systems, with obvious implications for vigilant and continuous monitoring.

ACKNOWLEDGEMENTS

This project is one of many outcomes of the Unzen Scientific Drilling Project (http://hakone.eri.u-tokyo.ac.jp/vrc/usdp/index.html), which continues to be co-operatively managed and supported at all stages by Kozo Uto and Hideo Hoshizumi of the Geological Survey of Japan (GSJ), and the Ministry of Education, Culture, Sports, Science, and Technology (MEXT). We are deeply appreciative to be involved in such a captivating project and are very grateful for the opportunity to have been granted access to the USDP cores, which are the property of the GSJ. Setsuya Nakada, University of Tokyo, kindly provided a sample from the andesite lava flow erupted from Unzen volcano in the year 1663. We thank Anita Grunder, Jun-Ichi Kimura, and Nelia Dunbar for their insightful and constructive reviews, and John Gamble for his final improvements. We also thank the following people for their helpful suggestions and thought-provoking discussions: George Bergantz, Carrie Browne, Alain Burgisser, Michelle Coombs, Gail Davidson, James Gardner, Nguyen Hoang, Pavel Izbekov, Jessica Larsen, Paul Layer, Setsuya Nakada, Christopher Nye, John Pallister, Jennifer Reynolds, Don Snyder, Yuki Suzuki, and Robert Wiebe. Ivan Belousov assisted with electron microprobe analyses of many pyroxenes and olivines, and we appreciate his involvement in this study. Ken Severin also assisted with electron microscopy, especially with respect to ensuring that the electron microprobe located at the University of Alaska Fairbanks Advanced Instrumentation Laboratory functioned properly. We are also especially grateful to Nobuo Geshi, Arata Kurihara, and Akikazu Matsumoto for their assistance and dedication during sampling at the USDP drill core storage facility in Tsukuba City. Finally, we express thanks to the National Science Foundation for their co-operation and patience, in addition to their financial support of this research (Grant EAR-0310406).

REFERENCES

Anderson, A. T., Jr, Swihart, G. H., Artioli, G. & Geiger, C. A. (1984). Segregation vesicles, gas filter-pressing, and igneous differentiation. *Journal of Geology* **92**, 55–72.

Anderson, D. J. & Lindsley, D. H. (1988). Internally consistent solution models for Fe–Mg–Mn–Ti oxides: Fe–Ti oxides. *American Mineralogist* **73**, 57–61.

Bacon, C. R. (1986). Magmatic inclusions in silicic and intermediate volcanic rocks. *Journal of Geophysical Research* **91**, 6091–6112.

Bacon, C. R. & Hirschmann, M. M. (1988). Mg/Mn partitioning as a test for equilibrium between coexisting Fe–Ti oxides. *American Mineralogist* **73**, 57–61.

Bacon, C. R. & Metz, J. (1984). Magmatic inclusions in rhyolites, contaminated basalts, and compositional zonation beneath the Coso volcanic field, California. *Contributions to Mineralogy and Petrology* **85**, 346–365.

Bacon, C. R., Bruggman, P. E., Christiansen, R. L., Clynne, M. A., Donnelly-Nolan, J. M. & Hildreth, W. (1997). Primitive magmas at five Cascade volcanic fields; melts from hot, heterogeneous sub-arc mantle. *Canadian Mineralogist* **35**, 397–423.

Chen, C., Nakada, S., Shieh, Y. & DePaolo, D. J. (1999) The Sr, Nd and O isotopic studies of the 1991–1995 eruption at Unzen, Japan. *Journal of Volcanology and Geothermal Research* **89**, 243–253.

Clynne, M. A. (1999). A complex magma mixing origin for rocks erupted in 1915, Lassen Peak, California. *Journal of Petrology* **40**, 105–132.

Clynne, M. A. & Borg, L. E. (1997). The composition of olivine and chromian spinel in primitive calc-alkaline and tholeiitic lavas from the southernmost Cascades Range, California: a reflection of relative fertility of the source. *Canadian Mineralogist* **35**, 453–472.

Coombs, M. C., Eichelberger, J. C. & Rutherford, M. J. (2002). Experimental and textural constraints on mafic enclave formation in volcanic rocks. *Journal of Volcanology and Geothermal Research* **119**, 125–144.

Criss, J. W. (1980). Fundamental parameters calculations on a laboratory microcomputer. *Advanced X-ray Analysis* **23**, 93–97.

Davidson, J., Tepley, F., Palacz, Z. & Meffan-Main, S. (2001). Magma recharge, contamination and residence times revealed by *in situ* laser

ablation isotopic analysis of feldspar in volcanic rocks. *Earth and Planetary Science Letters* **184**, 427–442.

Devine, J. D., Gardner, J. E., Brack, H. P., Layne, G. D. & Rutherford, M. J. (1995). Comparison of microanalytical methods for estimating H_2O contents of silicic volcanic glasses. *American Mineralogist* **80**, 319–328.

Didier, J. (1973). Granites and their enclaves; the bearing of enclaves on the origin of granites. *Developments in Petrology* **3**, 35–476.

Eichelberger, J. C. (1978). Andesitic volcanism and crustal evolution. *Nature* **275**, 21–27.

Eichelberger, J. C. (1980). Vesiculation of mafic magma during replenishment of silicic magma reservoirs. *Nature* **288**, 446–450.

Eichelberger, J. C., Gooley, R., Nitsan, U. & Rice, A. (1976). A mixing model for andesitic volcanism (abstract). *EOS Transactions, American Geophysical Union* **57**, 1024.

Eichelberger, J. C., Chertkoff, D. G., Dreher, S. T. & Nye, C. T. (2000). Magmas in collision; rethinking chemical zonation in silicic magmas. *Geology* **28**, 603–606.

Gill, J. B. (1981). *Orogenic Andesites and Plate Tectonics*. Berlin: Springer.

Heiken, G. & Eichelberger, J. C. (1980). Eruptions at Chaos Crags, Lassen Volcanic National Park, California. *Journal of Volcanology and Geothermal Research* **7**, 443–481.

Helz, R. T. (1979). Alkali exchange between hornblende and melt: a temperature sensitive reaction. *American Mineralogist* **64**, 953–965.

Holtz, F., Sato, H., Lewis, J., Behrens, H. & Nakada, S. (2005). Experimental petrology of the 1991–1995 Unzen dacite, Japan. Part 1: Phase relations, phase composition, and pre-eruptive conditions. *Journal of Petrology* **46**, 319–337.

Huppert, H. E., Sparks, R. S. J. & Turner, J.S. (1982*a*). Effects of volatiles on mixing in calc-alkaline magma systems. *Nature* **297**, 554–557.

Huppert, H. E., Turner, J. S. & Sparks, R. S. J. (1982*b*). Replenished magma chambers; effects of compositional zonation and input rates. *Earth and Planetary Science Letters* **57**, 345–357.

Hoshizumi, H., Uto, K. & Watanabe, K. (1999). Geology and eruptive history of Unzen Volcano, Shimabara Peninsula, Kyushu, SW Japan. *Journal of Volcanology and Geothermal Research* **89**, 81–94.

Hoshizumi, H., Uto, K., Matsumoto, A., Xu, S. & Oguri, K. (2002). Geology of Unzen volcano and core stratigraphy of the flank drilling (abstract). *Unzen Workshop 2002: International Workshop on the Unzen Scientific Drilling Project*, pp. 4–8.

Jaeger, J. C. (1968). Cooling and solidification of igneous rocks. In: Hess, H. H. & Poldervaart, A. (eds) *Basalts, Volume 2*. New York: John Wiley, pp. 503–536.

Jaupart, C. & Vergniolle, S. (1989). The generation and collapse of a foam layer at the top of a basaltic magma chamber. *Journal of Fluid Mechanics* **203**, 347–380.

Koyaguchi, T. & Blake, S. (1991). Origin of mafic enclaves; constraints on the magma mixing model from fluid dynamic experiments. Enclaves and granite petrology. *Developments in Petrology* **13**, 415–429.

Le Bas, M. J., Le Maitre, R. W., Streckeisen, A., *et al.* (1986). Chemical classification of volcanic rocks based on the total alkali–silica diagram. *Journal of Petrology* **27**, 745–750.

Le Maitre, R. W., Bateman, P., Dudek, A., Keller, J., Lemeyre, J., Le Bas, M. J., Sabine, P. A., Schmid, R., Sorensen, H., Streckeisen, A., Woolley, A. R. & Zanettin, B. (1989). *A Classification of Igneous Rocks and Glossary of Terms*. Oxford: Blackwell.

Lofgren, G. E. (1980). Experimental studies on the dynamic crystallization of silicate melts. In: Hargraves, R. B. (ed.) *Physics of Magmatic Processes*. Princeton, NJ: Princeton University Press, pp. 487–551.

Luhr, J. F. & Carmichael, I. S. E. (1985). Jorullo volcano, Michoacan, Mexico (1759–1774): the earliest stages of fractionation in calc-alkaline magmas. *Contributions to Mineralogy and Petrology* **90**, 142–161.

Melekestsev, I. V., Ponomareva, V. V. & Volynets, O. N. (1995). Kizimen volcano, Kamchatka—a future Mount St. Helens? *Journal of Volcanology and Geothermal Research* **65**, 205–226.

Miller, T. P., Chertkoff, D. G., Eichelberger, J. C. & Coombs, M. C. (1999). Mount Dutton Volcano, Alaska; Aleutian Arc analog to Unzen Volcano, Japan. *Journal of Volcanology and Geothermal Research* **89**, 275–301.

Miyashiro, A. (1974). Volcanic rock series in island arcs and active continental margins. *American Journal of Science* **274**, 321–355.

Nakada, S. & Motomura, Y. (1999). Petrology of the 1991–1995 eruption at Unzen; effusion pulsation and groundmass crystallization. *Journal of Volcanology and Geothermal Research* **89**, 173–196.

Nakada, S., Shimizu, H. & Ohta, K. (1999). Overview of the 1990–1995 eruption at Unzen. *Journal of Volcanology and Geothermal Research* **89**, 1–22.

Nakamura, M. & Shimakita, S. (1998). Dissolution origin and syn-entrapment compositional change of melt inclusion in plagioclase. *Earth and Planetary Science Letters* **161**, 119–133.

NEDO (New Energy Development Organization) (1988). *Western District of Unzen. Report on the Promotion and Development of Geothermal Energy* **15**, 1060 (in Japanese).

Pallister, J. S., Hoblitt, R. P., Meeker, G. P., Knight, R. J. & Siems, D. F. (1996). Magma mixing at Mount Pinatubo; petrographic and chemical evidence from the 1991 deposits. In: Newhall, C. G. & Punongbayan, R. S. (eds) *Fire and Mud; Eruptions and Lahars of Mount Pinatubo, Philippines*. Seattle, WA: University of Washington Press, pp. 687–731.

Phillips, J. C. & Woods, A. W. (2001). Bubble plumes generated during recharge of basaltic magma reservoirs. *Earth and Planetary Science Letters* **186**, 297–309.

Robinson, P., Spear, F. S., Schumacher, J. C., Laird, J., Klein, C., Evans, B. W. & Doolan, B. L. (1982). Phase relations of metamorphic amphiboles: natural occurrence and theory. In: Veblen, D. R. & Ribbe, P. H. (eds) *Amphiboles: Petrology and Experimental Phase Relations. Mineralogical Society of America, Reviews in Mineralogy* **9B**, 3–42.

Roeder, P. L. & Emslie, R. F. (1970). Olivine–liquid equilibrium. *Contributions to Mineralogy and Petrology* **29**, 275–289.

Sack, R. O., Carmichael, I. S. E., Rivers, M. & Ghiorso, M. S. (1980). Ferric–ferrous equilibria in natural silicate liquids at 1 bar. *Contributions to Mineralogy and Petrology* **85**, 116–132.

Sato, H., Holtz, F., Behrens, H., Botcharnikov, R. & Nakada, S. (2005). Experimental petrology of the 1991–1995 Unzen dacite, Japan. Part II: Cl/OH partitioning between hornblende and melt and its implications for the origin of oscillatory zoning of hornblende phenocrysts. *Journal of Petrology* **46**, 339–354.

Singer, B. S., Dungan, M. A. & Layne, G. D. (1995). Textures and Sr, Ba, Mg, Fe, K and Ti compositional profiles in volcanic plagioclase clues to the dynamics of calc-alkaline magma chambers. *American Mineralogist* **80**, 776–798.

Sisson, T. W. & Bacon, C. R. (1999). Gas-driven filter pressing in magmas. *Geology* **27**, 613–616.

Snyder, D. & Tait, S. (1995). Magma mingling in replenishment of magma chambers; comparison of fluid-mechanic experiments with field relations. *Contributions to Mineralogy and Petrology* **122**, 230–240.

Sparks, R. S. J. & Marshall, L. A. (1986). Thermal and mechanical constraints on mixing between mafic and silicic magmas. *Journal of Volcanology and Geothermal Research* **29**, 99–124.

Stimac, J. A. & Pearce, T. H. (1992). Textural evidence of mafic–felsic magma interaction in dacite lavas, Clear Lake, California. *American Mineralogist* **77**, 795–809.

Stimac, J. A., Pearce, T. H., Donnelly-Nolan, J. M. & Hearn, B. C., Jr (1990). The origin and implications of undercooled andesitic inclusions in rhyolites, Clear Lake Volcanics, California. *Journal of Geophysical Research* **95**, 17729–17746.

Stormer, J. C. (1983). The effects of recalculation on estimates of temperature and oxygen fugacity from analyses of multicomponent iron–titanium oxides. *American Mineralogist* **68**, 586–594.

Swanson, S. E. (1993). Crustal storage of andesite magma in the eastern Aleutian Arc (abstract). *Geological Society of America Annual Meeting* **25**, 327.

Tsuchiyama, A. (1985). Dissolution kinetics of plagioclase in the melt of the system: diopside–albite–anorthite, and origin of dusty plagioclase in andesites. *Contributions to Mineralogy and Petrology* **89**, 1–16.

Tsuchiyama, A. & Takahashi, E. (1983). Melting kinetics of a plagioclase feldspar. *Contributions to Mineralogy and Petrology* **84**, 345–354.

Ulmer, P. (1989). The dependence of the Fe^{2+}–Mg cation-partioning between olivine and basaltic liquid on pressure, temperature and composition; an experimental study to 30 kbars. *Contributions to Mineralogy and Petrology* **101**, 261–273.

Uto, K., Nakada, S., Hoshizumi, H. & Shimizu, H. (2002). Overview of the Unzen Scientific Drilling Project and the progress of its first phase (abstract V10/01P/A01-001). *International Union of Geodesy and Geophysics 2003 Meeting, Sapporo, Japan.*

Vernon, R. H. (1983). Restite, xenoliths and microgranitoid enclaves in granites. *Journal and Proceedings of the Royal Society of New South Wales* **116**, 77–103.

Vernon, R. H. (1984). Microgranitoid enclaves in granites; globules of hybrid magma quenched in a plutonic environment. *Nature* **309**, 438–439.

Venezky, D.Y. & Rutherford, M. J. (1999). Petrology and Fe–Ti oxide reequilibration of the 1991 Mount Unzen mixed magma. *Journal of Volcanology and Geothermal Research* **89**, 213–230.

Wiebe, R. A. (1994). Silicic magma chambers as traps for basaltic magmas: the Cadillac Mountain Intrusive Complex, Mount Desert Island, Maine. *Journal of Geology* **102**, 423–437.

Wiebe, R. A. & Collins, W. J. (1998). Depositional features and stratigraphic sections in granitic plutons: implications for the emplacement and crystallization of granitic magma. *Journal of Structural Geology* **20**, 1273–1289.

Wiebe, R. A., Blair, K. D., Hawkins, D. P. & Sabine, C. P. (2002). Mafic injections, *in situ* hybridization, and crystal accumulation in the Pyramid Peak Granite, California. *Geological Society of America Bulletin* **114**, 909–920.